UNCLASSIFIED

AD NUMBER: AD0894240

LIMITATION CHANGES

TO:

Approved for public release; distribution is unlimited.

FROM:

Distribution authorized to U.S. Government agencies only; Test and Evaluation; 19 May 1972. Other requests shall be referred to Space and Missile Systems Organization, Los Angeles, CA 90045.

AUTHORITY

SAMSO ltr dtd 31 Jul 1972

THIS PAGE IS UNCLASSIFIED

AD894240
AD No.
DDC FILE COPY

3SR-707
August, 1971

SYSTEMS, SCIENCE AND SOFTWARE

P.O. BOX 1620, LA JOLLA, CALIFORNIA 92037, TELEPHONE (714) 453-0060

THE DYNAMIC BEHAVIOR OF CONCRETE

H. E. Read and C. J. Maiden

DDC
RECEIVED
MAY 19 1972
A

TOPICAL REPORT

Prepared for

See 1473

SPACE AND MISSILE SYSTEMS ORGANIZATION
Air Force Systems Command
United States Air Force
Norton Air Force Base, California

Contract No. FO 4701-70-C-0194
Capt. J. H. Salch, Project Officer


ACCESSION for
WHITE SECTION
NTIS
BUFF SECTION
DDC
UNANNOUNCED
JUSTIFICATION
BY
DISTRIBUTION/AVAILABILITY CODES
DIST.
AVAIL. and/or SPECIAL
A

3SR-707
August, 1971

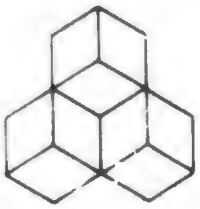

SYSTEMS, SCIENCE AND SOFTWARE

P.O. BOX 1620, LA JOLLA, CALIFORNIA 92037, TELEPHONE (714) 453-0060

THE DYNAMIC BEHAVIOR OF CONCRETE

H. E. Read and C. J. Maiden

TOPICAL REPORT

Prepared for

Distribution limited to U.S. Gov't. agencies only; Test and Evaluation; 19 MAY 1972. Other requests for this document must be referred to

SPACE AND MISSILE SYSTEMS ORGANIZATION
Air Force Systems Command
United States Air Force
Norton Air Force Base, California 92409
attn: MMNSS

Contract No. FO 4701-70-C-0194
Capt. J. H. Salch, Project Officer

Acknowledgements

The authors wish to express their appreciation to Mr. S. J. Green of Terra Tek, Dr. V. G. Gregson, Jr., of General Motors, and Dr. J.M. Shea of Physics International for supplying results and summaries of unpublished work and for many helpful discussions. The authors are indebted to the following members of the S^3 staff for valuable assistance in the course of this work: Mr. R. H. Fisher developed the program for treating the porous model in the RIP code, while Mrs. Janet Bishop, Mr. R. A. Cecil, and Mr. J. W. Wiehe provided assistance in the numerical studies.

Abstract

A review of the current knowledge of the dynamic behavior of concrete is given. Summaries of related research studies performed by the academic community and the following defense contractors are presented: Aerospace Corporation, General Motors, Gulf General Atomic, Physics International, Terra Tek, and TRW. Particular attention is given in this review to rapid, impulsive loading of concrete resulting from mechanical impact and sudden expcsure to radiation. Shock wave propagation and spallation phenomena are discussed. The coefficients for an existing constitutive model of a porous material are determined for a particular concrete. Numerical results based on this model and on an existing elastic-perfectly plastic model are given for several shock loading problems, and comparisons with corresponding experimental data are presented. The results indicate that neither model is adequate enough to predict with reasonable accuracy the shock effects in concrete. Recommendations for future research in these areas are given.

CONTENTS

1. INTRODUCTION

The successful function of many defense-related structures requires that they have the capability to survive a nuclear explosion without experiencing appreciable damage. Recently, some questions have arisen concerning the ability of several defense-related concrete structures to meet this requirement and, to address some of these questions, the present study was initiated.

Clearly, the most direct approach for evaluating the hardness of the structures in question would be to simply expose them to a reasonable nuclear environment and make post-test examinations for damage. Such an approach cannot, of course, be followed inasmuch as above-ground nuclear testing is prohibited and underground nuclear testing is impractical due to the enormous size of the concrete structures of interest. The use of smaller scale-models of the structures is also questionable inasmuch as the complex behavior of concrete does not lend itself to ordinary scaling procedures. Consequently, other means of evaluating the structural hardness of these structures must be employed and, to this end, attempts have been made to study their dynamic response and damage thresholds experimentally under simulated loading conditions produced by high explosives and by numerical calculations based on idealized mathematical models of the basic physical phenomena. For the most part, these approaches have not succeeded, to date, in providing credible answers to the question of structural hardness mentioned above.

The primary purpose of the present report is to provide a review of the current knowledge concerning the mechanical behavior of concrete, particularly in regard to rapid, impulsive loading, and to offer recommendations for future research in this area. Topics such as shock wave propagation and spallation are given special consideration. Current and prior

research programs related to the dynamic response characteristics of concrete are reviewed and discussed. Finally, coefficients for an existing constitutive model for porous materials are determined from experimental data reviewed in this report. Numerical results based on this model and on an existing elastic-plastic model are given for several shock loading problems, and comparisons with corresponding experimental data are presented.

2. PRELIMINARY CONSIDERATIONS

2.1 Structure of Concrete

Concrete is a composite material consisting of sand and coarse aggregate bonded together by a hardened cement paste. It is a multiphase material containing at least eight components, namely, coarse aggregate, sand, unhydrated cement, cement gel, gel pores, capillary pores, entrapped air voids, and free water.[1] The aggregate normally consists of either gravel or crushed rock, having a macroscopically nonuniform distribution of constituents. The hardened cement contains many flaws in the form of gel pores, capillary pores, and other voids filled with air or water. The resulting composite material is heterogeneous and very porous, typically containing a void volume in excess of 10 percent of the total volume. In addition to this, the cement gel consists of about 28 percent extremely fine pores, approximately 20 A^{o} in diameter, which can probably be ignored in the development of constitutive relations.

Through the use of x-ray photography and microscopy, considerable insight has been obtained into the internal structure of concrete.[2] With these methods it has been determined that small fissures or microcracks develop in concrete at the interface between coarse aggregate and mortar before it experiences any load. The presence of pre-existing microcracks is also reflected in the small concavity of the initial portion of the compression stress-strain curve.[3] The compaction process which results from the closure of the cracks produces a small increase in both the elastic modulus and ultrasonic pulse velocity. The pre-existing microcracks, termed "bond cracks," seem to result mainly from volume changes during hydration and drying. It appears, from the presence of these microcracks, that the interfacial bond is the weakest element in the concrete.

2.2 General Mechanical Properties

The mechanical properties of concrete have been investigated under a wide variety of loading conditions, but the majority of tests have been performed at quasi-static loading rates under either uniaxial or biaxial stress conditions. From the results of these studies, it has been found that concrete exhibits many of the salient response features also found in rocks, some of which are listed below:

- The nonlinear constitutive response of concrete is apparently due to the process of microcracking and pore closure, as well as the progressive breakdown of the internal structure of the material. Microcracks can develop from stress and strain concentrations resulting from the incompatibility of the elastic moduli of the aggregate, sand, and cement paste components.
- Under hydrostatic compression, concrete behaves reversibly (no permanent set) for pressures up to several ksi. At higher pressures, permanent changes take place in the microstructure and the behavior is no longer reversible.
- Concrete exhibits dilatancy, the property of a material to undergo increases in volume due to the action of shearing stresses. In both concrete and rocks, the dilatancy is apparently related to the extension and opening of small cracks in the material.
- The response of concrete is rate-dependent.[4] It appears that the rate-dependence stems from the fact that, on the microscale, the deformation process occurs mainly through the propagation of internal cracks. Consequently, as the rate of loading is increased, the time available for crack growth is

shortened and the material responds more like an intact (uncracked) solid. When the loading rate is very high, such as occurs in impact loading, the pre-existing cracks largely determine the dynamic response.

The method of manufacture can seriously affect the properties of concrete. For instance, segregation during casting can cause anisotropy, inadequate vibration during casting can drastically reduce strength, and too rapid drying can cause weakening through the formation of shrinkage cracks.

Finally, the hydration process between cement and water is slow and may not be completed for many years. Hence, the strength of concrete is continually increasing, though in most cases at least 90 percent of full strength has been reached in less than one year.

2.2.1 Effect of Composition

The mechanical properties of concrete are affected by the type of cement, volume fraction of cement, the water to cement ratio, the volume fraction of air voids, the type of aggregate, and the distribution and volume fraction of aggregate.

The strength of hardened cement and concrete increases significantly with a decrease in the water/cement ratio. For instance, the static modulus of elasticity can increase by a factor of 3 (from about 1×10^6 to 3×10^6 psi) as the water/cement ratio decreases from 0.60 to 0.30.[5] The ultimate strength is at least as dramatically affected by the water/cement ratio.[6]

Air voids also have a severely adverse effect on the strength of concrete. In this regard, the strength S of cement paste or concrete can be described by the relationship

$$S = f\left(\frac{V_c}{V_w + V_v}\right) \qquad (1)$$

where V_c, V_w, and V_v are the volume fractions of cement, water, and air voids, respectively. Thus, in general, strength increases with cement content and decreases with air and water content.

The type, volume fraction, and grading of aggregate in concrete can significantly affect the modulus of elasticity of concrete[7] (see Fig. 1). Essentially, the modulus of elasticity of the concrete increases or decreases with the volume fraction of aggregate, depending on whether or not the stiffness of the aggregate is greater or less than the stiffness of the cement. Also, it has been established that, with most natural aggregates, failure in concrete is initiated at the aggregate cement interface and that the shape, surface texture, and grading of the aggregate can have an effect on the strength. For instance, rough textured aggregate has been shown[8] to increase the strength of concrete. Furthermore, the flexural strength has been found to increase 10 percent as the maximum aggregate size increased from 3/4 to 2 1/2 in.[9] It should be noted that the strength of concrete is much more sensitive to the water/cement ratio than to aggregate type or volume fraction.

2.2.2 Effect of Testing Conditions

The typical stress-strain behavior of concrete under quasi-static uniaxial stress compression is shown in Fig. 2. The behavior is approximately linearly elastic up to a point (defined, say, as the point where there is a 0.2 percent deviation from linearity) which is analogous to the elastic limit in metals. This deviation from linearly elastic behavior occurs at stresses from 40-60 percent of the ultimate strength and is where significant bond failures at the aggregate-cement interface begin to be initiated. At stresses from

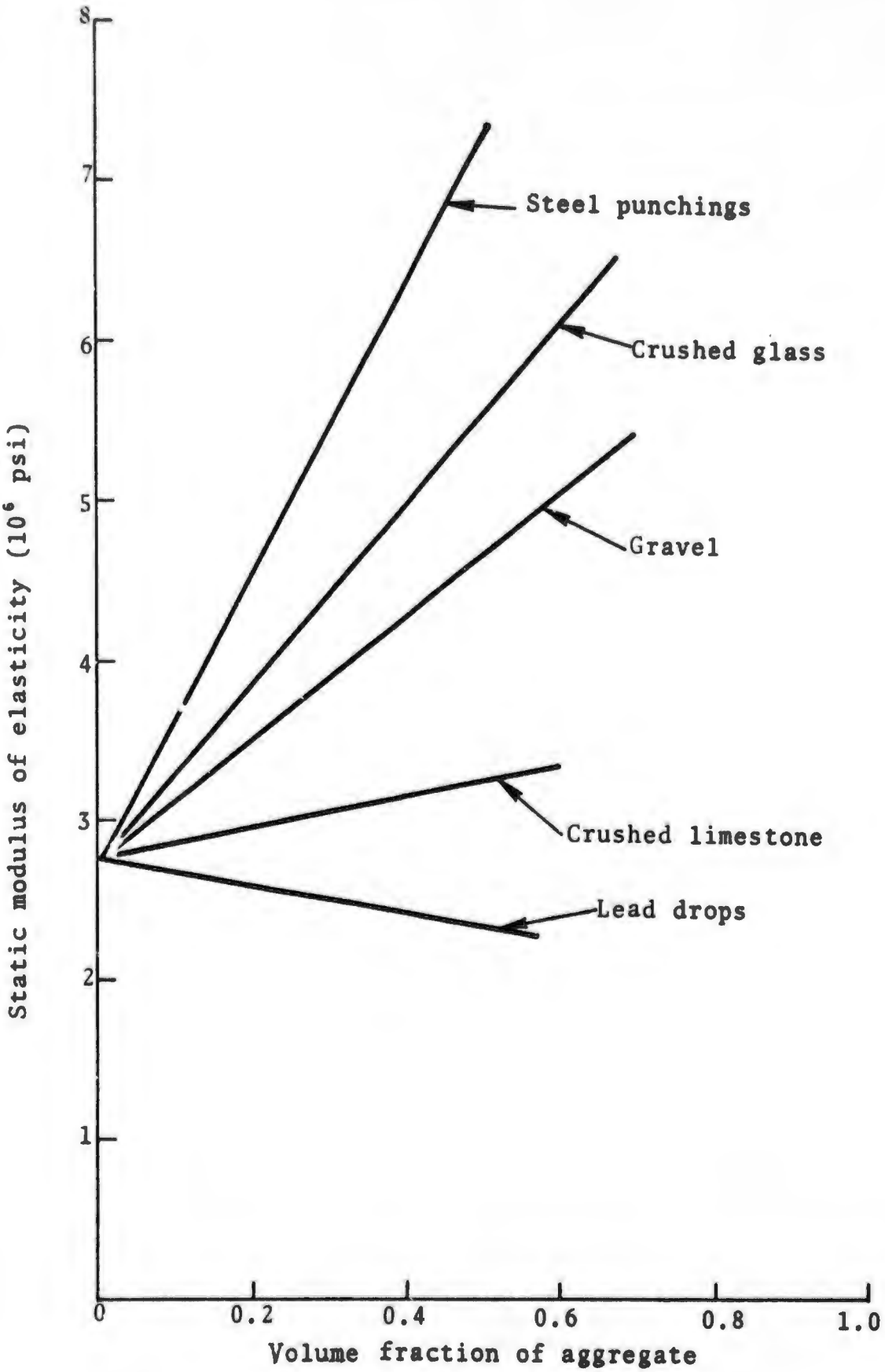

Fig. 1 - Static modulus of elasticity as a function of aggregate type and volume fraction (from Ref. 7).

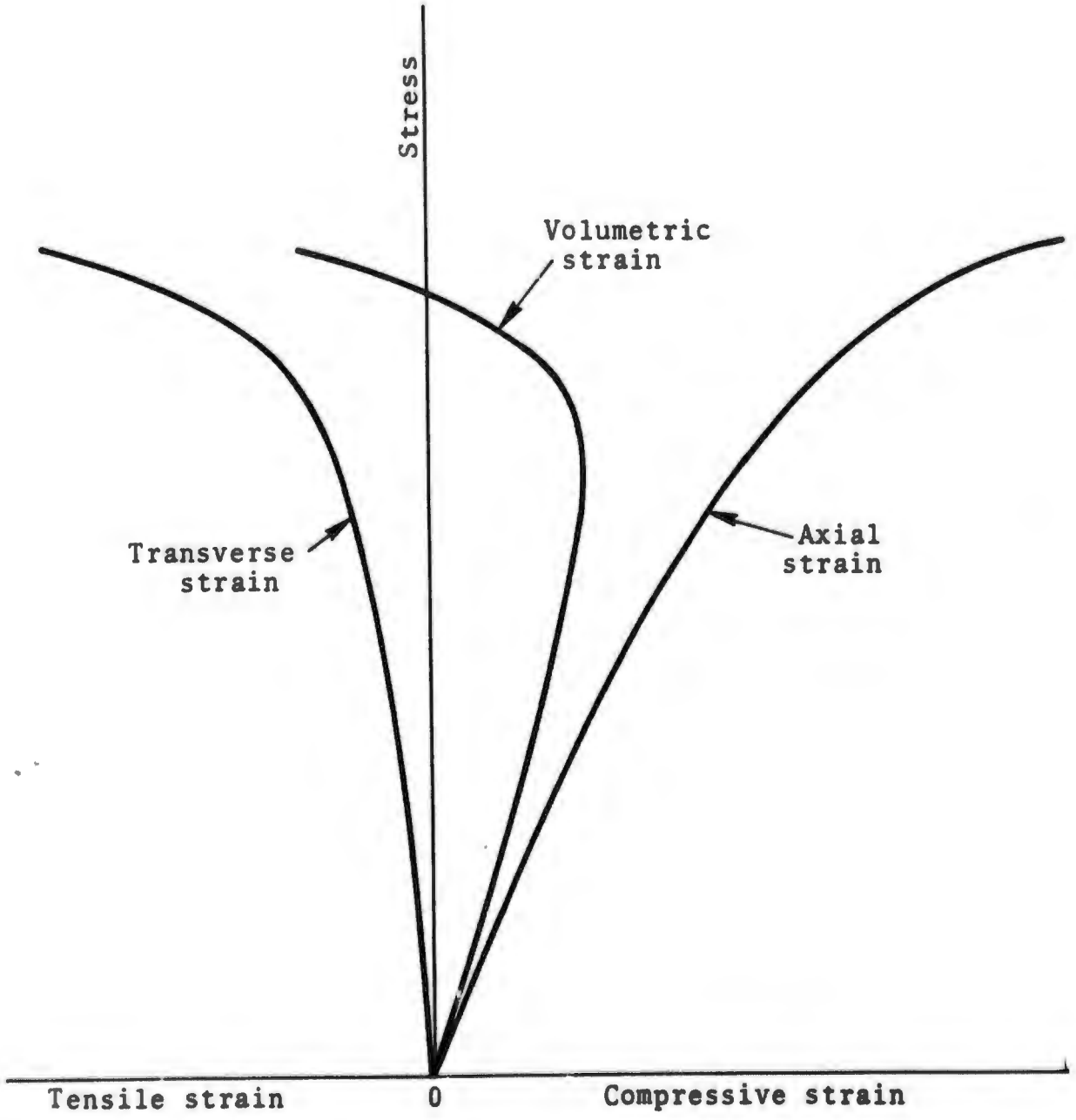

Fig. 2 - Typical stress-strain curves for concrete compressed under uniaxial stress.

about 70-90 percent of the ultimate strength, the specimen volume starts to increase (dilatancy) due to massive disruption of the internal structure.

The above stress-strain behavior can be modified by a number of factors in addition to the effect of composition discussed previously. Such factors are size of specimen, temperature, moisture content, rate of application of load, and state of stress and strain.

Concrete behaves as many brittle materials do in that apparent strength and variation of behavior decrease as the physical size of the specimen increases. This effect, which has been explained by the Griffith's crack or weakest link theories, is a relatively small one for concrete in that only a 25 percent decrease in strength has been observed for a volume increase of 5832 times.[10]

Testing temperature seems to have a significant effect on the strength of concrete in that a 1 percent decrease in strength has been observed for every 2°F increase in temperature between 25 and 130°F.[11] This means a 50 percent decrease in strength occurs over the above temperature range. This degradation in strength is at least partly due to cracking caused by the different thermal coefficients of expansion of aggregate and cement.

Moisture content is also important. Gently air-dried specimens have been found to give ultimate strengths 20-30 percent higher than for saturated specimens, although this difference might well increase significantly under multiaxial stress conditions (as has been observed in triaxial tests on Cedar City granite[12]).

Several investigations have been conducted to determine the effect of rate of loading on the stress-strain behavior of concrete. The results show that concrete is strain-rate sensitive.[4] The modulus of elasticity can increase 50 percent

and the ultimate strength 30-80 percent as the strain rate increases from about 10^{-3} to 10^{3} sec^{-1}.

At this time there is still no universally accepted criterion for failure of concrete under combined stresses. A considerable amount of data is available on the ultimate strengths of mortar and concrete under various conditions of combined stress; however, only a few data are available on stress or strain levels at the discontinuity point under multiaxial stress. Tentative surfaces of discontinuity and failure for concrete are suggested by Newman and Newman[13] but, as they caution, many more experimental results are required before the shapes of these surfaces can be confirmed.

3. DYNAMIC BEHAVIOR

In this section, the present state of knowledge regarding the dynamic behavior of concrete is summarized, including its response to both impulsive mechanical and radiative loading.* In addition, the capability of two constitutive models to describe stress wave propagation phenomena in this material is explored. The results of numerical studies of several stress wave propagation problems, recently investigated experimentally, are given for two constitutive models, namely, a Von Mises-type, elastic-plastic model which utilized material constants determined by TRW,[14] and a porous material model[15] for which the material constants were determined from data reviewed in this report. Comparisons are given between the numerical results for both constitutive models and corresponding experimental data.

3.1 Review of Earlier Work

A survey of the literature indicates that, compared with the numerous investigations of the static behavior of concrete, very little attention has been given to its dynamic behavior. Inasmuch as concrete apparently deforms through internal crack growth and degradation of the microstructure, significant differences are expected, however, between the static and dynamic properties. Of the few reported studies of concrete's dynamic behavior, most have been experimentally oriented, with only minor attention given to the development of a constitutive model of dynamic behavior.

3.1.1 Impulse Mechanical Loading

In 1966, Goldsmith, Polivka, and Yang[16] reported a study of the response of concrete to impact loading. Using a

*This review does not include (classified) studies of the response of concrete to nuclear radiation that have been carried out underground, nor the results of engineering and design studies of specific concrete structures.

Hopkinson bar technique, the propagation and attenuation of transient one-dimensional stress waves in cylindrical concrete specimens consisting of 1/4 in. aggregate were studied. Peak stresses on the order of 1/3 of a kilobar were obtained in the concrete propagated in a nondispersive manner and exhibited only a small degree of attenuation. From these observations, a solid-friction constitutive model was proposed to describe the dynamic behavior of concrete at the relatively low stress levels studied.

The results of a study of the dynamic behavior of concrete at stress levels substantially below those reported in Ref.16 were published in 1970 by Pozzo.[17] To investigate the nature of the internal friction mechanism of concrete, the decrement of small, free oscillations of concrete specimens was experimentally studied. From this investigation, Pozzo concluded that the solid-friction model provided a simple constitutive model of concrete at low stress levels, in agreement with the earlier results of Goldsmith et al.[16]

The dispersion of small elastic stress pulses in concrete has been investigated by Whittier and Ching.[18] Step pulses in the elastic range (70 psi) were produced in concrete specimens having 3/8 in. aggregate by shock tube loading. The shapes of the smeared pulses were observed at propagation distances of 2.4, 4.4, and 6.4 in. The authors found that the increase in the rise time with propagation distance was consistent with an elastic stochastic scattering wave model.

At higher stress levels, the most extensive study, to date, of stress wave propagation in concrete was done by Gregson.[19] Using a gas gun, Gregson experimentally determined the uniaxial strain response of concrete specimens to the impact of flyer plates, and attempted to define the shock Hugoniot of this material. Stresses produced in the concrete ranged from about 3 kbar to 552 kbar. At stresses below

25 kbar, the existence of a two-wave structure was confirmed and a relatively dispersive "elastic" precursor wave was observed. Many of the response features of the concrete (18 percent porosity) observed by Gregson were typical of a porous solid, such as, for example, the dependence of the shock velocity on the particle velocity, as shown in Fig. 3. Although Gregson's study was not extensive enough to thoroughly map out the dynamic properties of concrete, it provides a general indication of the behavior of this material over a wide range of stresses, strains, and strain rates, and can serve as a starting point in the development of a realistic constitutive model.

A limited experimental study of the uniaxial strain response of concrete to shock loading performed by Gulf General Atomic is summarized in Ref.20. High explosives were used to produce impulse loads in several concrete specimens. The experiments were performed on regular 3/4-in. aggregate concrete specimens, as well as on specimens containing 3 percent entrained air. Stress histories at depths of 2, 4, and 6 in. from the loading surface were obtained experimentally. The measured stresses in the air entrained samples at depths of from 2 to 6 in. from the loading surface ranges from 0.92 to 1.1 kbar; for the same loading conditions, the stresses in the regular samples ranged from 0.56 to 0.59 kbar.* In all cases, no significant attenuation was observed beyond a depth of 2 in.

In addition to standard concretes, Hugoniot measurements have been reported for several special concrete materials, such as mortar,[21] Fondu Fyre,[19] and epoxy resin grouts.[22] A comparison of the experimentally determined Hugoniot data for these materials with the standard concrete data from Ref. 19 is shown in Fig. 4, where the dependence of the shock velocity on the particle velocity is depicted. As this figure reveals, there is good agreement between the data for a typical concrete,

*The large differences between the attenuated stress levels for the regular and the air-entrained concrete observed in these experiments were unexpected and they have not, as yet, been satisfactorily explained on physical grounds.

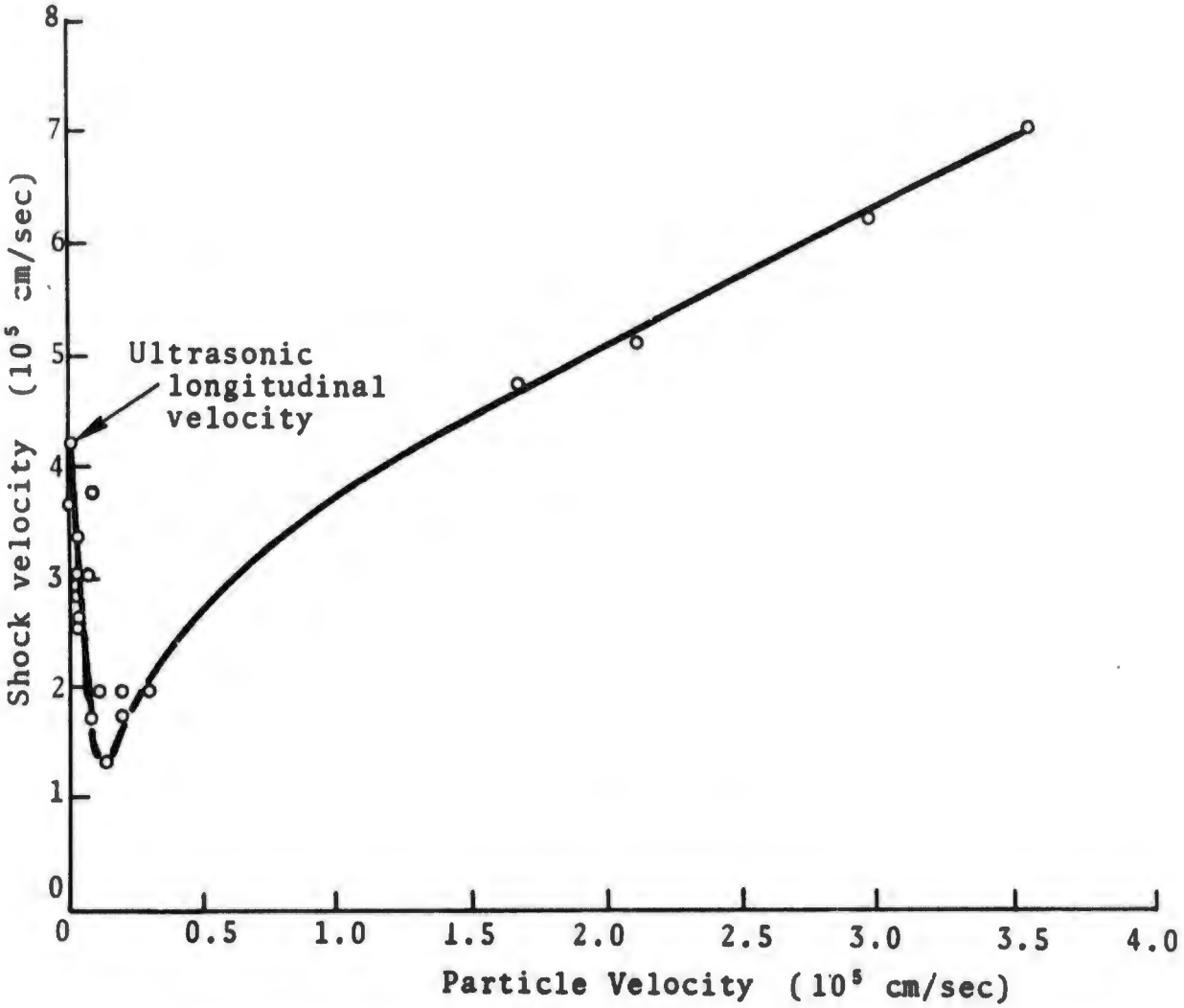

Fig. 3 - Shock velocity vs. particle velocity for 1/8-in. aggregate concrete (from Ref. 19)

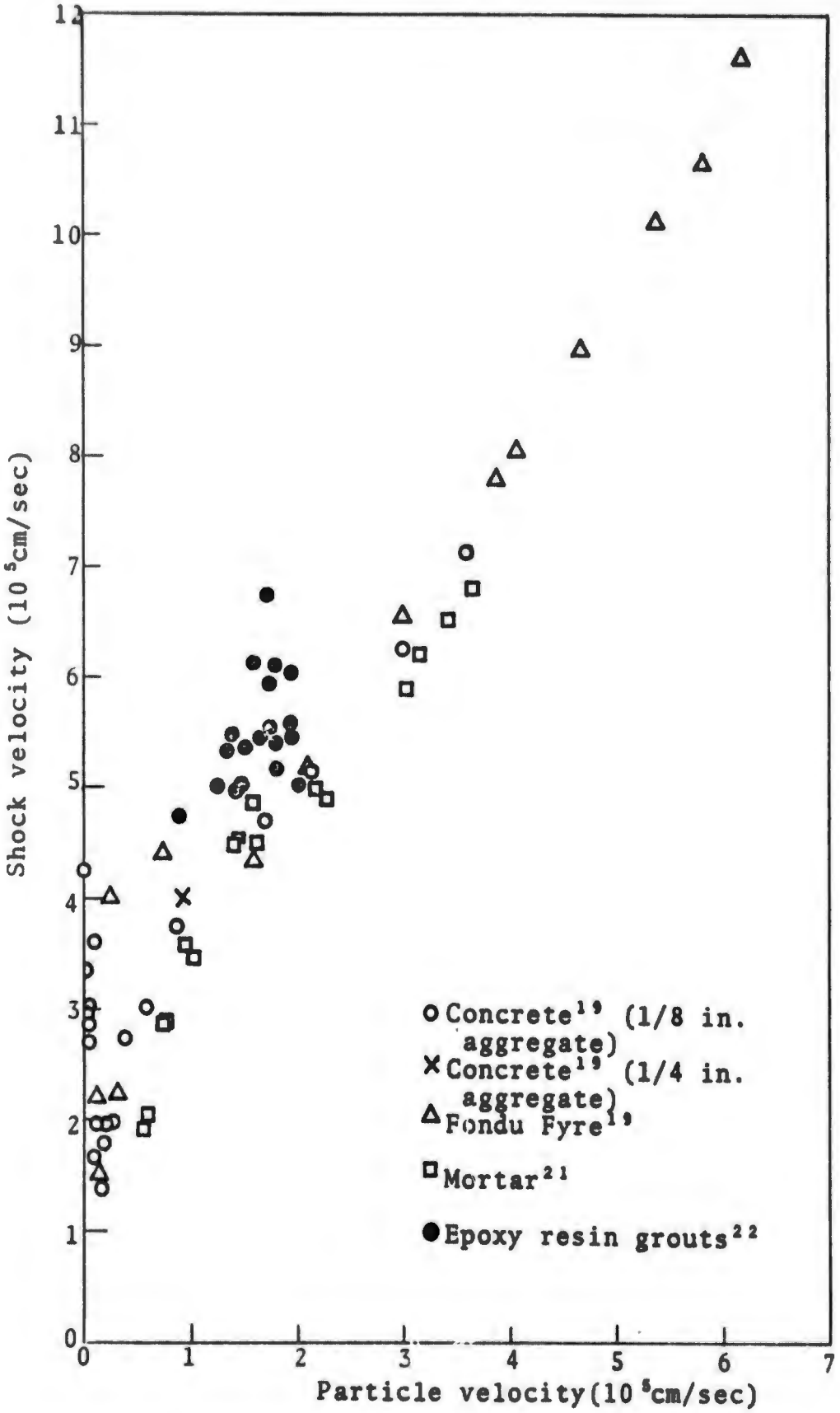

Fig. 4 - Comparison of Hugoniot data for several concrete materials.

Fondu Fyre, and mortar for particle velocities greater than about 1×10^5 cm/sec; below this value of the particle velocity, there is considerable scatter in the data due partly to the complications in analysis introduced by the presence of a smeared two-wave structure. Finally, the data for the epoxy resin grouts fall substantially above that for the other materials considered in this figure.

3.1.2 Radiation-Induced Impulsive Loading

Aside from the (classified) studies of the response of concrete to radiative energy carried out underground,[14,23] the only attempt at a systematic determination of the Grüneisen coefficient in the laboratory was made by Shea[24] at Physics International.† In this experimental program,* slabs of concrete were irradiated by an electron beam with a mean energy of 1 meV and a pulse duration of 40 nsec. Sample thicknesses were on the order of 1/8 in. thick, which is slightly greater than the maximum range of the electrons. An x-cut quartz transducer was bonded to the rear surface of the concrete to measure the compressive stress pulse that resulted from the energy deposition. Material response calculations, based upon the known energy deposition, and the Hugoniot for the sample material were performed using various assumed values for the Grüneisen coefficient until the measured and computed values agreed.

Two types of concrete were tested. One type consisted of high strength (6000 psi unconfined compressive strength), low porosity concrete with ∿ 1/16 in. granite aggregate prepared by Waterways Experimental Station (WES). The other concrete was prepared by Testing Engineers, Inc., of Oakland, California, using fine aggregate only (98 percent passing

†The peak induced stress in these experiments was less than 1 kbar.

*This summary of the (unpublished) work at Physics International was prepared at the author's request by Dr. J. Shea for inclusion in this section.

No. 16 sieve), with an unconfined compressive strength of 4000 psi and an air entrainment admixture that produced 9 percent porosity.

The results are presented in Fig. 5; for the WES concrete they give a value of 0.080 ± 0.01 for the Grüneisen coefficient. The air-entrained material was initially expected to yield a lower Grüneisen coefficient, since porosity generally produces this effect; however, the experimental results give a value of 0.15 ± 0.02.

The most plausible explanation for this difference appears to be the moisture content. The WES material was cored from slabs and shipped dry to Physics International; several months elapsed between the time the samples were prepared until they were irradiated, during which time they were stored dry in the laboratory. On the other hand, only a few days elapsed between the time the air-entrained concrete finished its 28-day cure (100 percent humidity) and when it was tested. Consequently, it is expected that the moisture content of these samples is much greater.

3.1.3 Spallation

In the experiments performed by Gulf General Atomic discussed earlier, some limited information about spallation of concrete was obtained, although no attempt was made to determine spall thresholds. It was found that, for an incident stress having a magnitude between 3 and 5 kbar, spallation occurred in the regular concrete specimens but not in the air-entrained specimens. Thus, the spall threshold for air-entrained concrete must be notably higher than for standard concrete. A high-speed photographic process for recording the breakup of concrete following spallation as utilized in part of this program, and some photographs of the breakup process of the regular concrete specimens are given in Ref. 20.

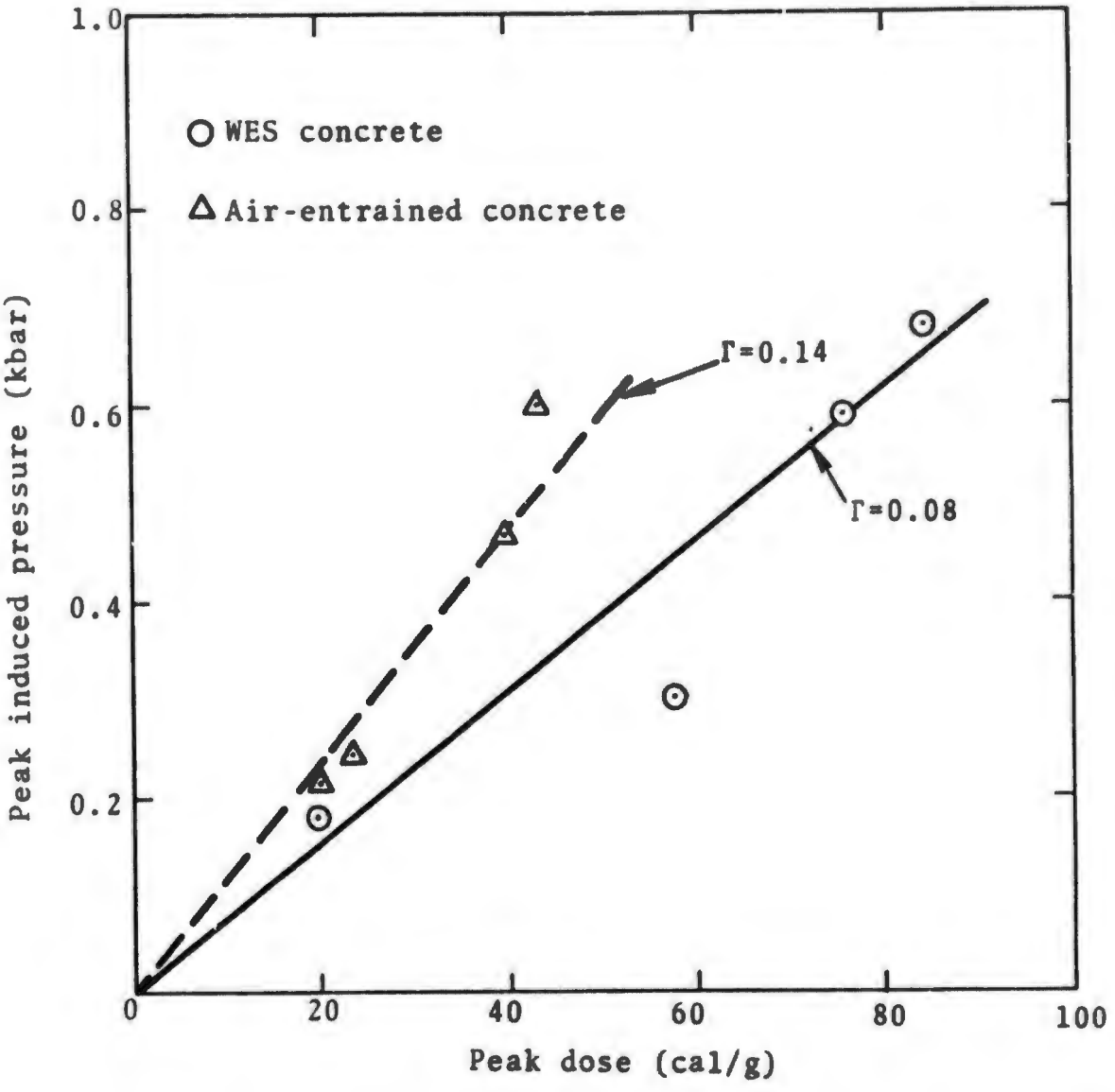

Fig. 5 - Pulsed electron beam energy-pressure coupling results on concrete (from Ref. 24)

Using the pulsed electron beam, Shea obtained a limited amount of spall data on oven-dried and water-saturated concrete.[24] The experimental configuration employed entailed sudden uniform heating of a slab, so the tensile state is formed by stress relief waves from both free surfaces that meet in the midplane of the sample. The threshold for complete spall was found to lie between 27 and 37 cal/g for dry concrete. Only a few shots were made on water-saturated concrete, with spall observed at a dose of 16 cal/g. Front-surface spall data were obtained in the Grüneisen experiment, but generally the data were either well above or well below the threshold.

Birkimer and Lindemann have studied the dynamic tensile strength of several types of concrete under uniaxial stress conditions.[25] Plane waves were produced in long prismatical concrete specimens by the impact of high velocity projectiles. A spall criterion was developed from theoretical grounds which predicted that the critical fracture strain should vary as the one-third power of the strain rate. The results of the experiments supported the proposed theoretical spall criterion over the range of strain rates investigated. In the case of plain concrete, a maximum strain rate of 25 sec^{-1} was obtained.

3.1.4 Other Related Studies

At Terra Tek, Green et al. are currently pursuing a combined theoretical and experimental program to develop a realistic constitutive model of concrete.[26] Primary attention has been given to the low strain rate and low stress level behavior of concrete, with the goal of developing a constitutive model appropriate for use in structural interaction codes. In the experimental phase of this program, a systematic study of hydrostatic and multiaxial stress behavior has been made. Quasi-static deformation of cylindrical 3/8 in. aggregate specimens has been investigated for stress up to 4 kbar. The separate influences of the hydrostat and the

deviatoric stress component have been isolated. Figure 6 shows the observed behavior of concrete under pure hydrostatic loading. Here, the variation of the mean normal stress, σ_m, with volume changes is depicted. The mean normal stress is defined as the average of the three principal stress components, σ_i, i.e.,

$$\sigma_m = \frac{1}{3}(\sigma_1 + \sigma_2 + \sigma_3) \tag{2}$$

and, for pure hydrostatic loading, it is synonomous with the pressure. In Fig. 7, the dependence of the generalized deviatoric stress on the generalized deviatoric strain is shown for both loading and unloading at several values of confining pressure. In this figure, the generalized deviatoric stress, $\sqrt{J_2'}$, and the generalized deviatoric strain, $\sqrt{I_2'}$, are defined as follows:

$$\sqrt{J_2'} = \frac{1}{\sqrt{6}} \left| (\sigma_1 - \sigma_2)^2 + (\sigma_2 - \sigma_3)^2 + (\sigma_3 - \sigma_1)^2 \right|^{\frac{1}{2}}$$

$$\sqrt{I_2'} = \frac{1}{\sqrt{6}} \left| (\varepsilon_1 - \varepsilon_2)^2 + (\varepsilon_2 - \varepsilon_3)^2 + (\varepsilon_3 - \varepsilon_1)^2 \right|^{\frac{1}{2}} \tag{3}$$

where σ_i and ε_i denote principal components of stress and strain, respectively. The data from the experimental effort are now being used in the development of a constitutive model based on an extension of the capped yield surface approach which accounts for the effects of pore closure and dilatancy.

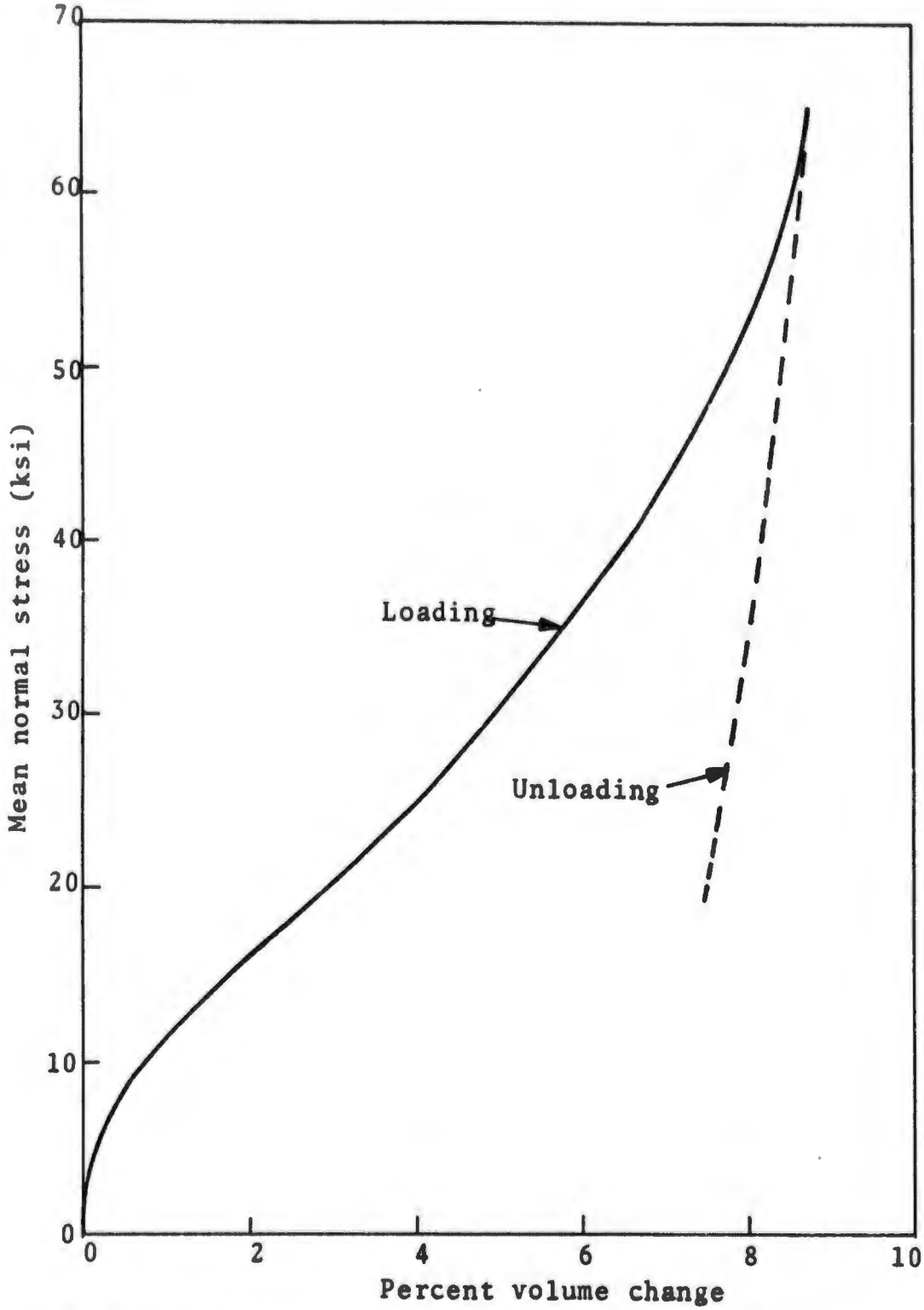

Fig. 6 - Behavior of concrete under pure hydrostatic loading (from Ref. 26)

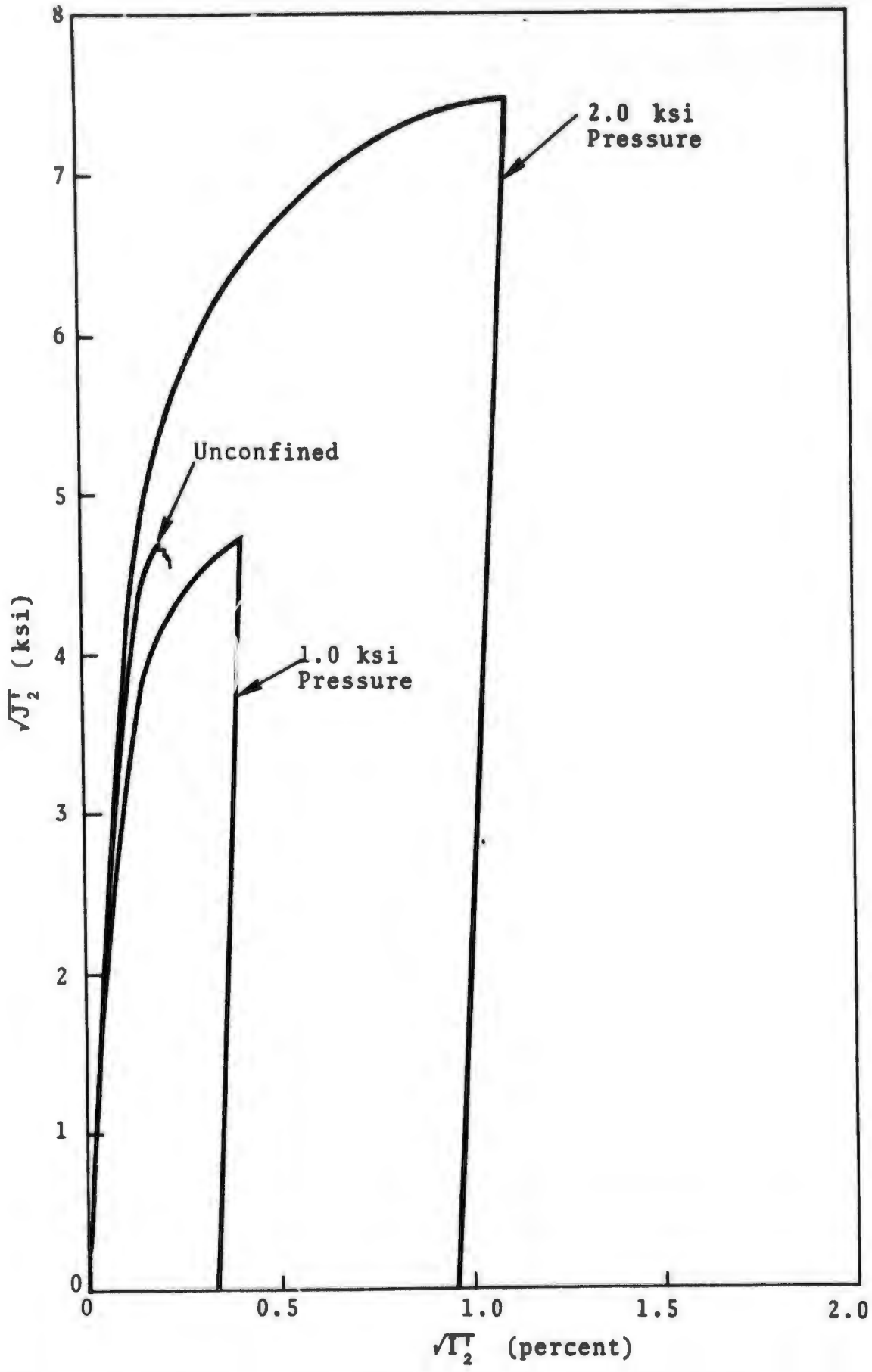

Fig. 7 - Generalized deviatoric stress vs. generalized deviatoric strain for several values of confining pressure (from Ref. 26).

3.2 Numerical Study of Stress Wave Propagation

Numerical studies of several stress wave propagation problems considered experimentally by Gregson[19] were performed using two theoretical constitutive models of concrete. One of the constitutive models, a von Mises elastic-plastic representation, has been frequently used by TRW[14] in analysis of underground test data. The other constitutive model, a P-α porous model,[15] for which the material parameters were determined from experimental data reviewed in this report, is included to explore the feasibility of using a simple porous model for describing the dynamic behavior of concrete. All of the numerical calculations reported in this section were performed with the one-dimensional, Lagrangian, finite-difference RIP code.[27] For each problem investigated in the present study, numerical results were obtained for both of the constitutive models mentioned above, and these are compared with the corresponding experimental results obtained by Gregson.

3.2.1 Description of Problems Investigated

From the wave propagation problems investigated by Gregson,[19] seven were selected for numerical study in the present work. The problems consisted of impulsively loading concrete specimens by impacting flyer plates at high velocity and determining the dynamic response of the concrete. In each case, the concrete specimens were backed by either Plexiglas, polyethylene, or X-cut quartz, depending on the type of information to be extracted during the experiment. In some of the experiments, stress history measurements were made at particular locations through the use of X-cut quartz gages or manganin wire gages embedded in the backup material. In other experiments, the laser interferometer was used to measure the particle velocity histories at positions in the backup material. The concrete specimens were supplied by the U.S. Army Waterways Experiment Station and contained 1/8 in. aggregate; they had a measured nominal density of 2.19 g/cm^3 and a porosity of 18 percent. The nominal density of solid (nonporous)

concrete was 2.67 g/cm^3. The specific details of the problems selected for numerical study in the present work are given below in Table I.

Table I

Summary of Impact Problems Studied Numerically

Problem No.	Impact Velocity (cm/sec)	Flyer Plate	Target
1	3.93×10^4	Fused quartz 0.6499 cm thick	0.6416 cm concrete backed by 0.6363 cm X-cut quartz
2	4.13×10^4	6061-T6 aluminum 1.271 cm thick	1.2723 cm concrete backed by 0.6375 cm X-cut quartz
3	3.00×10^4	Lexan 0.95 cm thick	0.64 cm concrete backed by 1.9 cm of Plexiglas
4	3.88×10^4	"	" "
5	5.00×10^4	6061-T6 aluminum 1.27 cm thick	0.644 cm concrete backed by 3.48 cm of polyethylene
6	8.00×10^4	"	" "
7	13.50×10^4	"	" "

The constitutive equations for 6061-T6 aluminum, X-cut quartz, Plexiglas, and polyethylene given in Ref. 28 were used in the numerical calculations. Fused quartz was described by the constitutive equation given in Ref. 29 . General Motors supplied information on the constitutive properties of Lexan from which the following Hugoniot was determined:

$$\sigma = A\mu + B\mu^2 + C\mu^3 \qquad (4)$$

Here, σ denotes the stress, ρ is the density, $\mu = \rho/\rho_o - 1$, and

$$\rho_o = 1.20 \text{ g/cm}^3$$
$$A = 80 \text{ kbar}$$
$$B = 120 \text{ kbar}$$
$$C = 55 \text{ kbar.}$$

A description of the two constitutive models of concrete used in the numerical calculations is given in the following sections.

3.2.2 Elastic-Perfectly Plastic Constitutive Model

Material constants for a simple elastic-perfectly plastic constitutive model for use in conjunction with one-dimensional PUFF-type computer codes were determined by TRW.[14] In this representation concrete is modeled as a von Mises elastic-plastic body, in which shear strength effects are accounted for, but strain hardening and strain rate effects, as well as any Bauschinger effect or porosity are neglected. The stress σ is decomposed into a hydrostatic pressure component, P, and a deviatoric component, S:

$$\sigma = P + S \qquad (5)$$

The hydrostat is assumed to be reversible and the pressure P is described by a Mie-Grüneisen form of the equation of state normally used in connection with nonporous metals, namely,

$$P = (A\mu + B\mu^2 + C\mu^3)\left(1 - \frac{\Gamma_o \mu}{2}\right) + \Gamma_o \rho E \qquad (6)$$

where

$$\mu = \rho/\rho_o - 1 \qquad (7)$$

In Eq. (6), E denotes the specific internal energy and ρ_o, the initial density, has the value

$$\rho_o = 2.14 \text{ g/cm}^3$$

which differs by about 2 percent from the initial density of 2.19 g/cm³ determined by Gregson.[19]

The constants A, B, and C appearing in Eq. (6) are assigned the following values:

$$A = 255 \text{ kbar}$$
$$B = 233 \text{ kbar}$$
$$C = 943 \text{ kbar}$$

while the Grüneisen coefficient, Γ_o, is taken as

$$\Gamma_o = 2.3$$

The term "Grüneisen coefficient" is used here loosely in connection with the porous materials, such as concrete, and should actually be viewed as an "effective Grüneisen coefficient". In addition, it should be noted that the form of Eq. (6) tacitly assumes that the Grüneisen coefficient for (porous) concrete remains constant and does not vary with the density.

The deviatoric component of stress, S, reflects the shear strength and plastic effects in this constitutive model; it is described by the following expression·

$$S = \begin{cases} 4/3G \ln (\rho/\rho_o), & \text{for } |S| \leq 2/3 Y_o \\ \pm 2/3 Y_o, & \text{otherwise} \end{cases} \tag{8}$$

where G, the shear modulus, and Y_o, the yield stress in simple tension, are assigned the values

$$G = 202 \text{ kbar}$$
$$Y_o = 0.275 \text{ kbar}$$

Finally, it is noted that the above constitutive model of concrete rests on the assumption that the plastic, or anelastic,

portion of the deformation is incompressible; such an assumption is realistic for nonporous, crystalline solids but is clearly incorrect for a porous material, such as concrete. Furthermore, the above model assumes that the deviatoric components of stress are unaffected by the hydrostatic pressure; this assumption is clearly in disagreement with the experimental data obtained by Green et al.[26] (see Fig. 7) as well as others.

3.2.3 Porous Constitutive Model

Preliminary results of an attempt to utilize a porous constitutive model to describe concrete are reported in this section. The constitutive model is based on an idealized (and possibly untenable) concept of the deformational behavior of concrete in which shear strength effects are neglected, and the principal process governing the deformation of the concrete is assumed to be the closure (or opening) of preexisting pores.* The model describes the main features of the pore collapse process by empirically relating the state of the porous concrete to the corresponding state of nonporous concrete at the same pressure and temperature. The experimental data obtained by Gregson[19] are used to determine material parameters for this model. The general formulation is based on ideas originally proposed by Herrmann,[15] primarily in connection with a different class of porous materials, however, and the reader is referred to Ref. 15 for a detailed discussion of the basic approach.

3.2.3.1 Formulation of Model

Consider a deformable, solid material which, on the macroscopic level, contains a uniform distribution of pores

*It has not been established that pore collapse is the principal mechanism that governs the uniaxial strain deformation of concrete in the stress range of interest to the present study, i.e., up to 70 kbar. For uniaxial and biaxial states of stress, there is considerable evidence to indicate that concrete deforms through the propagation and opening of cracks.

and is isotropic and homogeneous. This material undergoes a deformation which produces uniaxial strain on a macroscopic level, but due to the pores, results in multiaxial strain on a microscopic level. In formulating a constitutive model for such a material, reference will be made to the equation of state of the corresponding nonporous (solid) material, and this will be assumed to be known and given in the form

$$P = f(v_s, E) \tag{9}$$

where P denotes the pressure, v_s is the specific volume of the solid material, and E represents its specific internal energy. In the present formulation, it is assumed that the solid material follows a Mie-Grüneisen form of the equation of state, in which case the function f is given by

$$f = P_H + \frac{\Gamma}{v_s}(E - E_H) \tag{10}$$

where P_H and E_H denote the pressure and specific internal energy, respectively, along the Hugoniot and Γ is the Grüneisen coefficient. Over a wide range of behavior, the pressure, P_H, along the Hugoniot can be represented in the form

$$P_H = A\mu + B\mu^2 + C\mu^3 \tag{11}$$

where

$$\mu = v_{so}/v_s - 1$$

and v_{so} denotes the specific volume of the solid material in the initial state. By making use of the Rankine-Hugoniot jump conditions, it can be shown that the combination of Eqs. (9), (10), and (11) leads to the following expression for the equation of state of the solid material:

$$P = (A\mu + B\mu^2 + C\mu^3)\left[1 - \frac{\Gamma_o \mu}{2(1+\mu)}\right] + \frac{\Gamma_o E}{v_{so}} \tag{12}$$

if it is assumed that the Grüneisen coefficient Γ varies with the specific volume v_s according to the equation

$$\Gamma = \Gamma_o \, (v_s/v_{so}) \tag{13}$$

where Γ_o denotes the value of the Grüneisen parameter in the initial, uncompressed state.

In order to distinguish the portion of the volume change in the porous material due to compression from that due to collapse of pores, it is expedient to introduce a porosity parameter, α, defined as

$$\alpha = v/v_s \tag{14}$$

where v is the specific volume of the porous material, and v_s is the specific volume of the solid (nonporous) material at the same pressure and temperature. Generally speaking, the parameter α will depend upon the full thermodynamic state of the porous material; in the present formulation, however, α will be taken to depend only on the pressure, that is,

$$\alpha = g(P) \tag{15}$$

which, as noted in Ref. 15, is equivalent to assuming that the mechanical behavior is insensitive to relatively small temperature changes, in addition to those normally experienced along the Hugoniot. Specific functional forms for the function $g(P)$ are selected to fit experimental results.

On the basis of the above considerations, the equation of state of the porous material is given by

$$P = f(v/\alpha, E) \tag{16}$$

where f is the same function that appears in Eq. (9), and the pressure P denotes a force per unit of total area of the porous material. An alternate formulation in which the pressure is defined as the force per unit of solid area has been given by Holt, Carroll, and Kusubov.[30]

Bearing in mind the specific form of the function f given in Eq. (10) for the solid material, the corresponding equation of state for the porous material, according to Eq. (16), is given by the expression

$$P = (A\mu+B\mu^2+C\mu^3)\left[1 - \frac{\Gamma_o\mu}{2(1+\mu)}\right] + \frac{\Gamma_o E}{v_{so}} \qquad (17)$$

where μ is now expressed in the form

$$\mu = \alpha \frac{v_{so}}{v} - 1 \qquad (18)$$

When taken together, Eqs. (15), (17), and (18) completely specify the equation of state of the porous material.*

*Inasmuch as the porous model described here neglects effects due to shear strength, it is physically meaningful only in the response regime where stresses are sufficiently high for deviatoric stress components to be neglected and yet not high enough to produce complete compaction. Clearly, such a model cannot be expected to provide a realistic description of mechanical behavior at low stresses, where shear strength effects are expected to be important.

Consider the dependence of the porosity parameter α on the pressure P. For a small deformation near α_o, the initial value of the porosity parameter in the unstrained state, it is reasonable to assume that concrete behaves in an elastic manner. For pressures below the elastic limit, P_y, it will be assumed that α depends linearly on the pressure, that is,

$$\alpha = \alpha_o + \alpha_o' P \tag{19}$$

Here α_o' is a constant which, as shown in Ref. 28, can be defined in terms of K_{so}, the bulk modulus of the solid material in the unstrained state, C_{so}, the corresponding bulk wave velocity in the unstrained solid material, and C_o, the wave velocity in the unstrained porous material, in the following manner:

$$\alpha_o' = \frac{\alpha_o}{K_{so}} \left(1 - \alpha_o \frac{C_{so}^2}{C_o^2} \right) \tag{20}$$

For pressures greater than P_y, the material responds anelastically. Permanent changes take place in the substructure as the pores close irreversibly. Anelastic behavior occurs for α in the range $1 \leq \alpha \leq \alpha_y$, where α_y is the value of the porosity parameter at the limit of elastic behavior. Within this range, α will be taken to depend on the pressure P in the form

$$\alpha = \exp\left[\sum_{n=0}^{m} a_n \, (\ell n \, P)^n \right] \tag{21}$$

where the a_n are constants. To be acceptable on physical grounds, the expression for α given in Eq. (21) must satisfy the condition $d\alpha/dP < 0$ for $P_y < P < P_s$, where P_s denotes the pressure at which the porous solid becomes fully compacted. Furthermore, to ensure that the transition from the porous condition to the fully compacted state occurs continuously and

smoothly, we shall require that Eq. (21) satisfy the condition $d\alpha/dP = 0$ for $P = P_s$. The constants a_n are then selected to fit experimental results, as well as the above conditions.

In the current form of the present model, unloading from a compressed state takes place at a constant value of α. Thus, if the material has been compressed to, say, $\alpha = \alpha_1$, α remains fixed at α_1 during the unloading process. A more realistic approach would permit α to change during the unloading process in such a manner that the sound velocity changed smoothly from its initial value of C_o to its final value of C_s in the fully compacted state; this refinement has not been incorporated into the present model, however, primarily due to the lack of sufficient experimental data on unloading and release wave phenomena in concrete.

3.2.3.2 Experimental Data and Evaluation of Coefficients

The experimental data obtained from the plate impact experiments reported in Ref. 19 have been processed by Gregson, using the Rankine-Hugoniot jump conditions, to give the results listed in Table II.* The results given in this table for the low stress level experiments should be viewed, however, only as approximate, inasmuch as there is considerable uncertainty as to whether or not the stress waves attained steady states, a tacit assumption upon which the Rankine-Hugoniot jump conditions rest.

Consider, first, the determination of the Hugoniot of the solid concrete. It seems reasonable to assume that, at pressures above 170 kbar, concrete will be fully compacted. Therefore, it will be assumed that the experimental data in Table II for stresses from 173 to 552 kbar lie on the Hugoniot of solid concrete. Using a third order, least squares fit to these data, and constraining the resulting curve to pass through the initial specific volume of the solid concrete, $v_{so} = 0.374\ cm^3/g$, leads

*Because of difficulties involved in the interpretation of the results from the direct impact experiments, the data given in Ref. 19 for these shots have not been included in Table II.

Table II

Hugoniot Data for 1/8 In. Aggregate Concrete (from Ref. 19)

Initial Density (g/cm^3)	Stress (kbar)	Density (g/cm^3)	Specific Volume (cm^3/g)	Shock Velocity (mm/μsec)	Particle Velocity (mm/μsec)
2.150	0.75	2.157	0.4637	3.60	0.01
2.150	22.0	2.490	0.4016	2.75	0.375
2.165	37.5	2.680	0.3732	3.02	0.58
2.158	70.75	2.810	0.3559	3.75	0.87
2.179	2.4	2.205	0.4535	3.02	0.036
	3.4	2.316	0.4319	1.628	0.096
	1.8	2.203	0.4538	2.70	0.030
	4.9	2.464	0.4058	1.40	0.162
	2.3	2.206	0.4532	2.89	0.036
	7.6	2.449	0.4084	1.78	0.196
	1.0	2.190	0.4566	2.98	0.015
	8.1	2.412	0.4145	1.96	0.190
	1.0	2.188	0.4571	3.39	0.014
	11.4	2.511	0.3983	1.99	0.263
	4.8	2.309	0.4331	1.98	0.111
2.150	173.0	3.381	0.2958	4.70	1.71
2.189	241.0	3.750	0.2667	5.14	2.14
2.153	407.0	4.142	0.2420	6.28	3.01
2.166	552.0	4.363	0.2292	7.12	3.58

to the following values for the coefficients A, B, and C:

$$\begin{aligned} A &= 1{,}134 \text{ kbar} \\ B &= -2{,}878 \text{ kbar} \\ C &= 3{,}909 \text{ kbar} \end{aligned} \tag{22}$$

Here, A may be identified as the bulk modulus of solid concrete at zero pressure, K_{so}. Using this information, and the value for ρ_{so} of 2.67 g/cm^3 given earlier, the initial sound velocity in the solid concrete, C_{so}, is found to be 6.53×10^5 cm/sec.

Now consider the specification of the P-α relationship for the porous concrete. In the elastic regime, α depends linearly on P according to Eq. (19). On the basis of such a relationship, elastic behavior can be completely specified by the initial value of the porosity parameter, α_o, the pressure at the limit of elastic behavior, P_y, and the slope of the α-P curve, α_o'. Using the values given earlier for the initial specific volumes of the porous and solid concrete, one finds $\alpha_o = 1.222$. The experimental studies by Gregson indicate that the elastic precursor in concrete, although relatively dispersive, transmits a stress of about 1 kbar; on the basis of this observation, we take*

$$P_y = 1 \text{ kbar} \tag{23}$$

The slope of the α-P curve, α_o', can be evaluated from Eq. (20), using the preceding information, once C_o, the initial bulk velocity in the porous concrete, has been specified. Unfortunately, no experimental information on C_o for concrete was available. Ultrasonic measurements of the longitudinal wave velocity, C_L, in concrete were reported in Ref. 19 and indicated that $C_L = 4.25 \times 10^5$ cm/sec. In the absence of more accurate information, then, the bulk sound velocity, C_o, will be assumed to have the same value as the measured longitudinal velocity. On this basis, evaluation of Eq. (20) leads to the following

*The notation P_y is used here since the deviatoric component S_y is not specifically accounted for in the model.

result:

$$\alpha_o' = -500 \text{ kbar} \quad . \tag{24}$$

The pressure, P_s, at which the porous concrete becomes fully compacted, is taken to be 120 kbar. The anelastic behavior in the crush region from P_y = 1 kbar to P_s = 120 kbar will be described by Eq. (21) with m = 3. Thus, the dependence of α on the pressure P in this region of behavior is taken in the form:

$$= \exp[a_o + a_1 \ln P + a_2 (\ln P)^2 + a_3 (\ln P)^3] \tag{25}$$

The constants a_o, a_1, a_2, and a_3 were evaluated to satisfy the conditions:

$$\frac{d\alpha}{dP} = 0 \quad , \quad \text{at } P = P_s$$

$$\frac{d\alpha}{dP} < 0 \quad , \text{ for } P_y < P < P_s$$

as well as to provide a fit to the experimental data given in Table II in the stress range 1-120 kbar. Proceeding in this manner, the following values for the constants were obtained:

$$\begin{aligned} a_o &= 1.988 \times 10^{-1} \text{ kbar} \\ a_1 &= -1.280 \times 10^{-2} \text{ kbar} \\ a_2 &= -2.012 \times 10^{-2} \text{ kbar} \\ a_3 &= 2.959 \times 10^{-3} \text{ kbar} \end{aligned} \tag{26}$$

The Hugoniots of the solid concrete and the crush curve of the porous concrete calculated, respectively, from Eqs. (12) and (17) using values for the coefficients listed in this section, are depicted in Fig. 8 together with the corresponding experimental data from Table II. A more detailed view of the solid Hugoniot, crush curve, and experimental data for

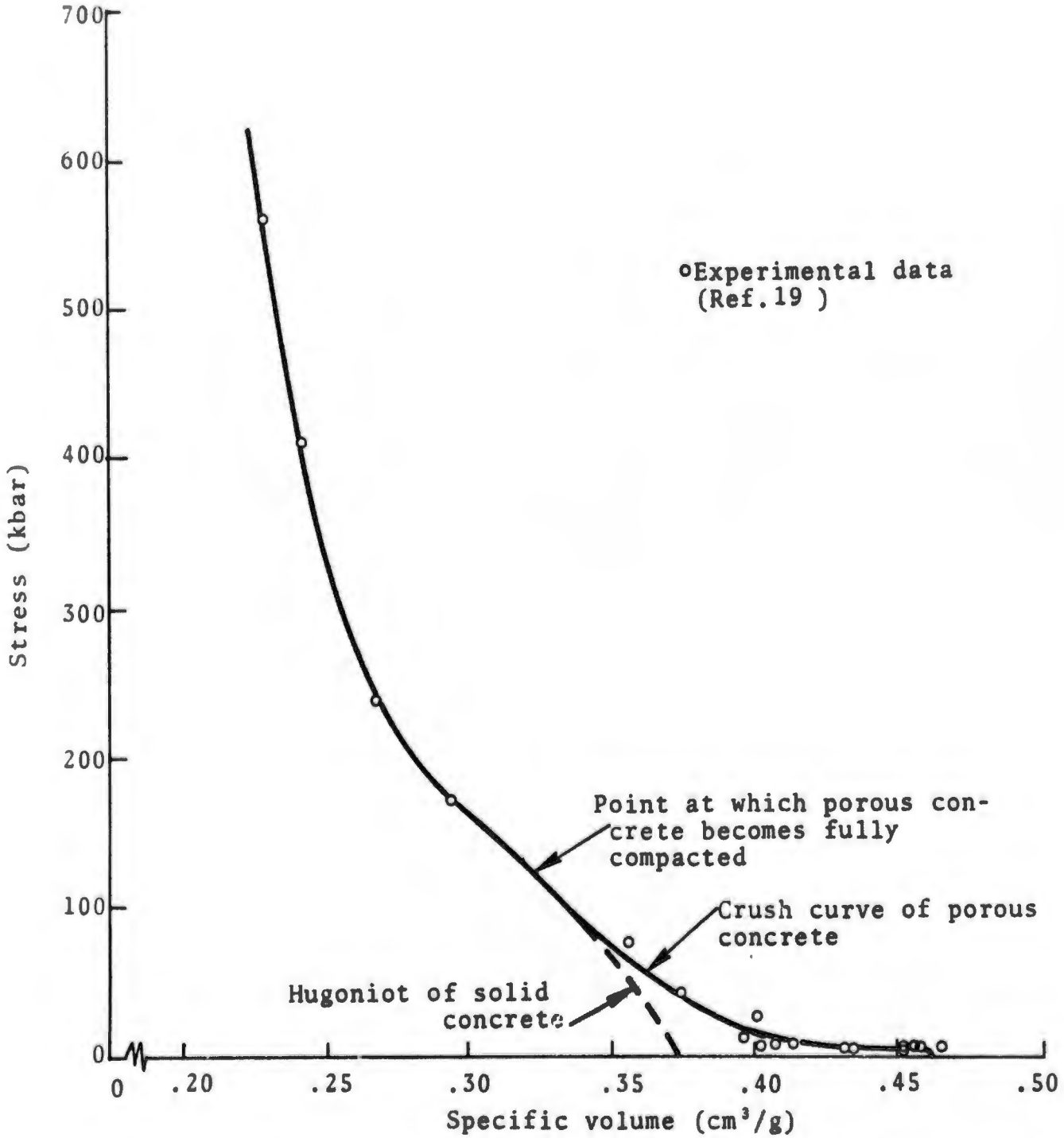

Fig. 8 - Theoretical and experimental Hugoniots of concrete in the stress range from 0 to 600 kbars.

stresses below 24 kbar is given in Fig. 9. From an inspection of this figure, it becomes evident that, due to the relatively large degree of scatter in the experimental data, a precise determination of the crush curve is not possible based solely on these data.

Finally, the Grüneisen coefficient is assigned the following value for concrete

$$\Gamma_o = 0.1 \tag{27}$$

in accord with the experimental results obtained by Shea.[24]

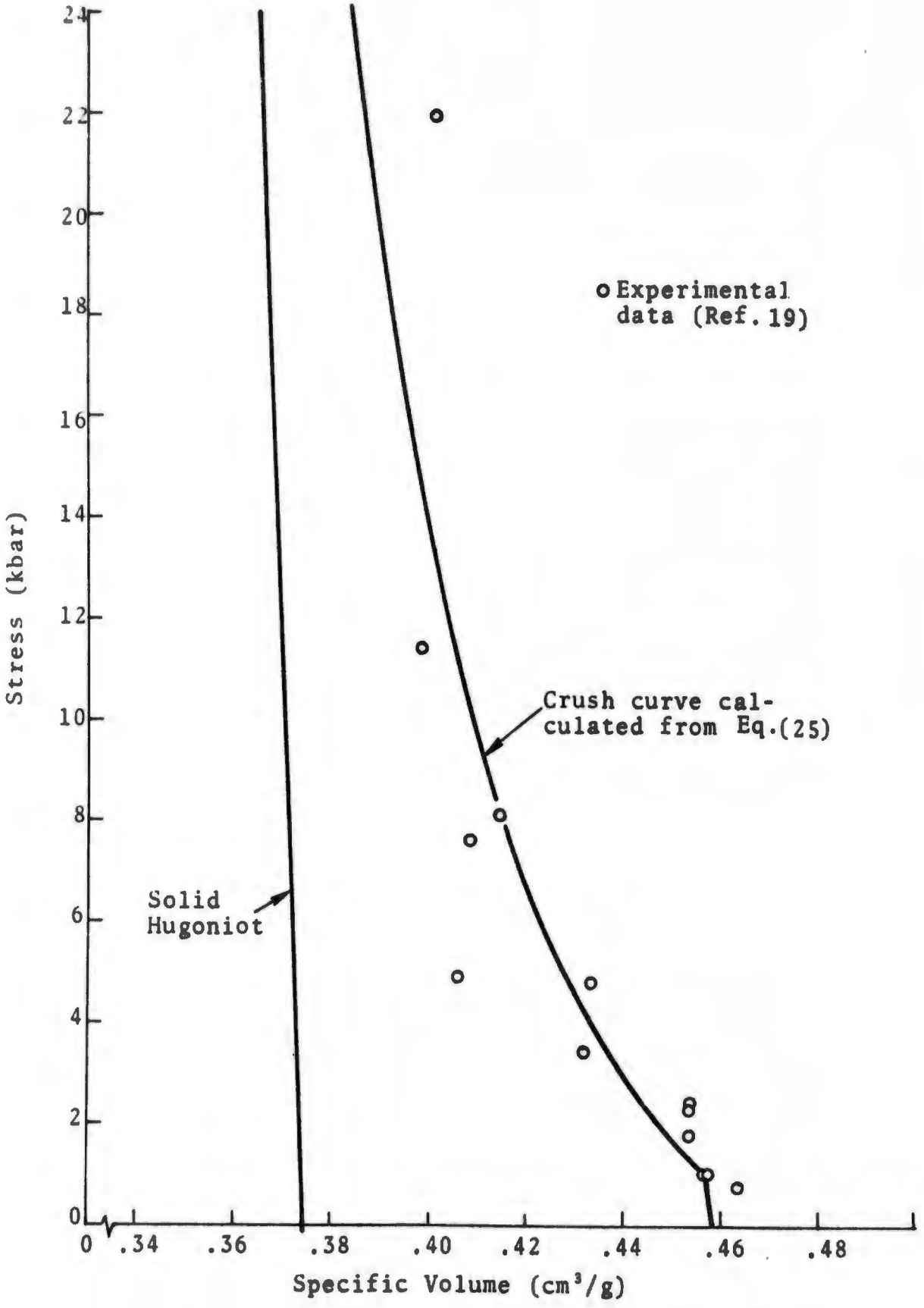

Fig. 8 - Theoretical and experimental Hugoniots of conrete in the stress range from 0 to 24 kbars.

3.2.4 Numerical Results

The results of the numerical studies of the problems listed in Table I are given in Figs. 10 to 16. The numerical calculations were carried out with the one-dimensional, Lagrangian, finite-difference RIP code using the elastic-perfectly plastic model and the porous model discussed in the preceding sections.

When comparing the experimental and calculated results, there are several things that one should keep in mind. First of all, in order to give an accurate portrayal of the TRW elastic-perfectly plastic model of concrete, no changes were made in the model described in Ref. 14. Consequently, in the calculations made with this model, an initial density of 2.14 g/cm^3 was used, while an initial density of 2.19 g/cm^3 was employed in the calculations performed with the porous model. Such a small difference in initial densities (about 2 percent) is not expected to introduce noticeable effects, however. Secondly, the accuracy of the numerical solutions depends not only on the constitutive model used for concrete but equally as well on the constitutive models employed to describe the other materials, namely, quartz, 6061-T6 aluminum, polyethylene, Plexiglas, and Lexan. While the response of quartz and 6061-T6 aluminum have been well characterized over the stress range of interest in the present study, the same is not altogether true for polyethylene, Plexiglas, and Lexan; these materials are known to have complex response characteristics over the stress range of interest* and, in the present calculations relatively simple representations of these materials were used due to the current absence of more sophisticated models.

*Barker, for example, has found that Plexiglas (PMMA) behaves as a viscoelastic material for stresses up to about 7 kbar; above this, it responds as an elastic-plastic rate-dependent material.[29]

Figures 10 and 11 depict the calculated and observed stress histories in concrete using the X-cut quartz gages. Experimental stress histories were determined for times greater than the normal recording time of the quartz gages by special procedures which involved accounting for the multiple reflections which occurred in the gages; such a technique, nevertheless, becomes increasingly less accurate as the recording time increases. In addition, no attempt was made to account for the influence of lateral rarefactions on the gages at late times due to the complex geometry. As a result, some uncertainty exists in the plastic wave profiles shown in these figures. It has been estimated,* however, that the experimentally determined peak amplitudes are correct to within 2 to 4 kbar, and that the observed arrival times are accurate to within 100 nsec. An inspection of Figs. 10 and 11 reveals that large discrepancies exist between the calculated and experimental results. The experimental data show that the stress waves have undergone appreciable attenuation during propagation through the concrete while the calculations indicate that no attenuation has occurred; in the stress histories based on the porous model, however, it is apparent that wave attenuation is imminent in both figures. In addition, the observed stress waves are considerably more smeared than those that were calculated, indicating the presence of additional effects not accounted for in the models, such as, for instance, strain rate effects and geometrical dispersion.

Figures 12 and 13 show the calculated and experimental results for Problems 3 and 4. Here, the particle velocity histories in the Plexiglas window material at a depth of 0.303 cm from the concrete-Plexiglas interface are depicted. The experimental particle velocity histories portrayed in these figures were obtained with a laser interferometer. Precise arrival times of the waves were not determined in the experiments; consequently, the experimental records were positioned in the figures so that the experimental arrival times coincided

*Private communication with W.M. Isbell, General Motors Corp.

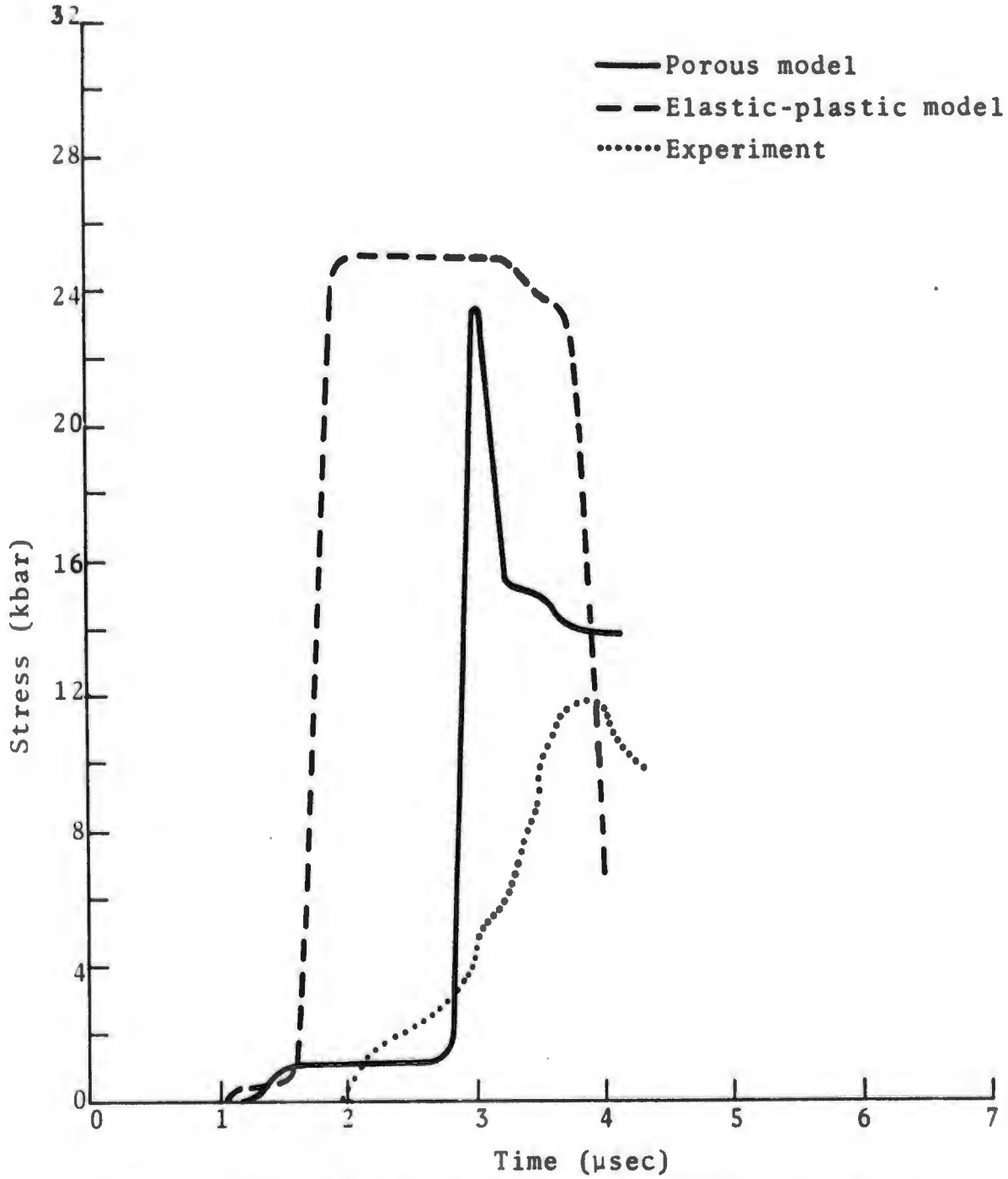

Fig. 10 - Stress histories at X-cut quartz--concrete interface for Problem No.1

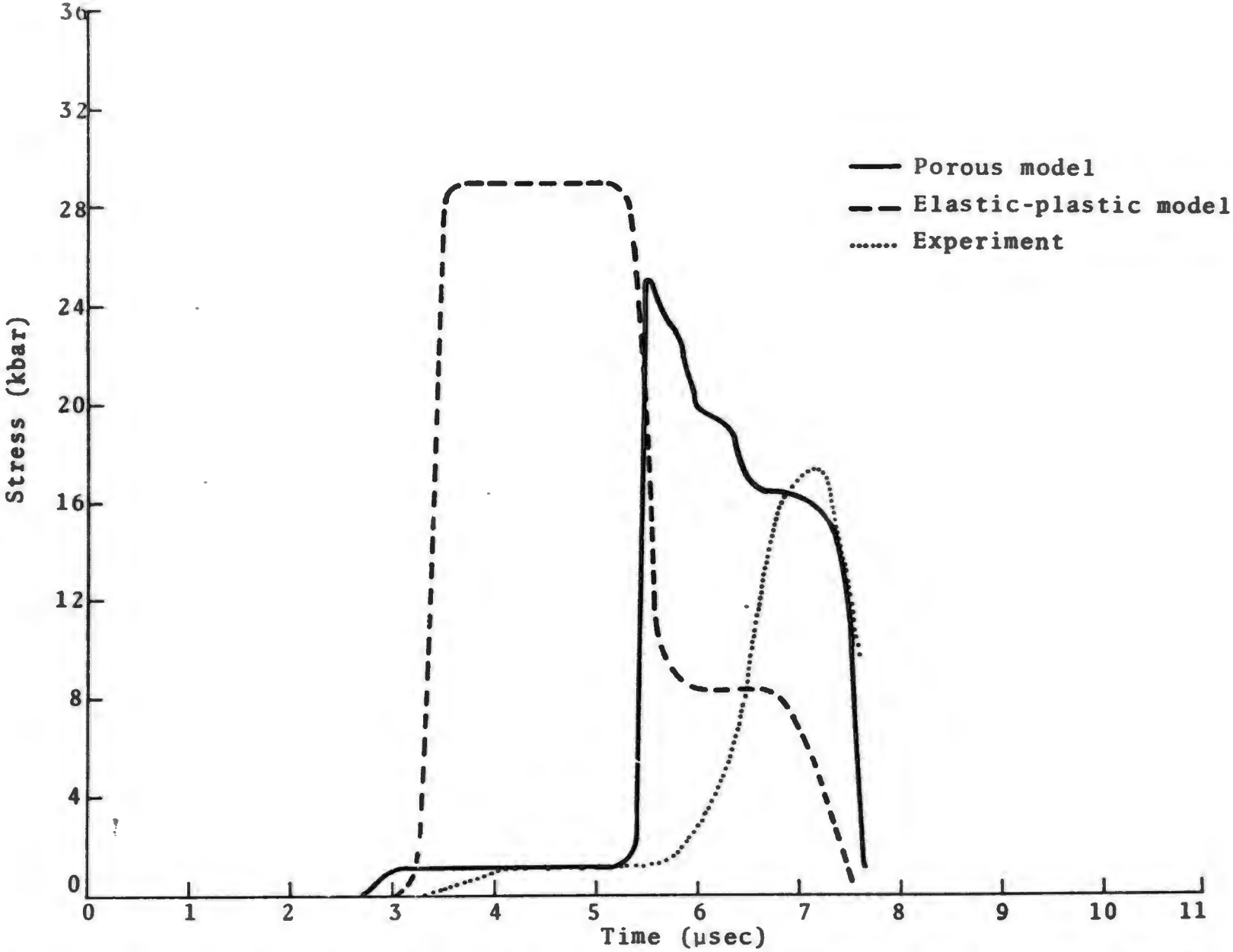

Fig.11 - Stress histories at X-cut quartz--concrete interface for Problem No. 2.

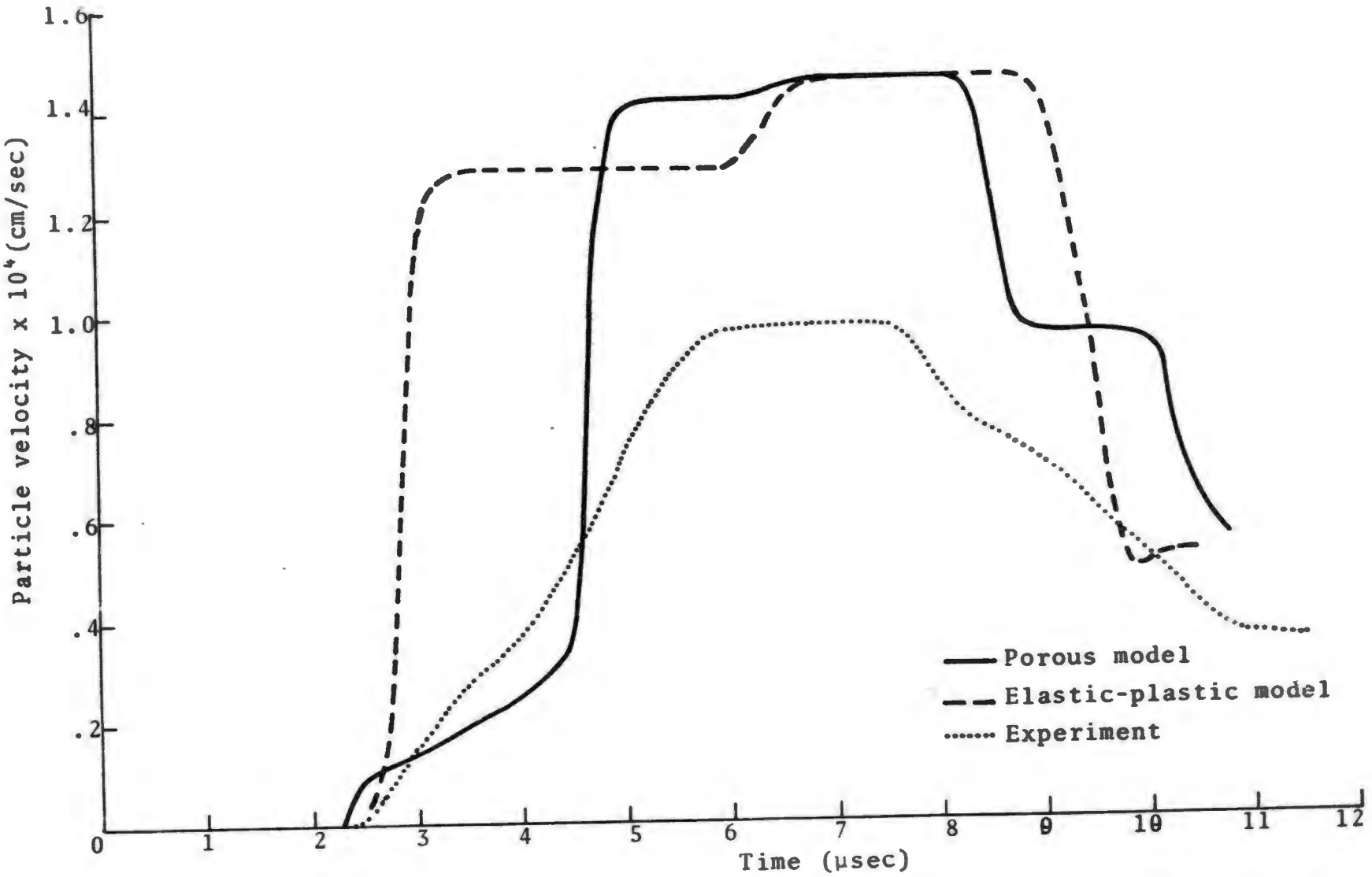

Fig.12 - Particle velocity histories at 0.303-cm depth in Plexiglas for Problem No.3

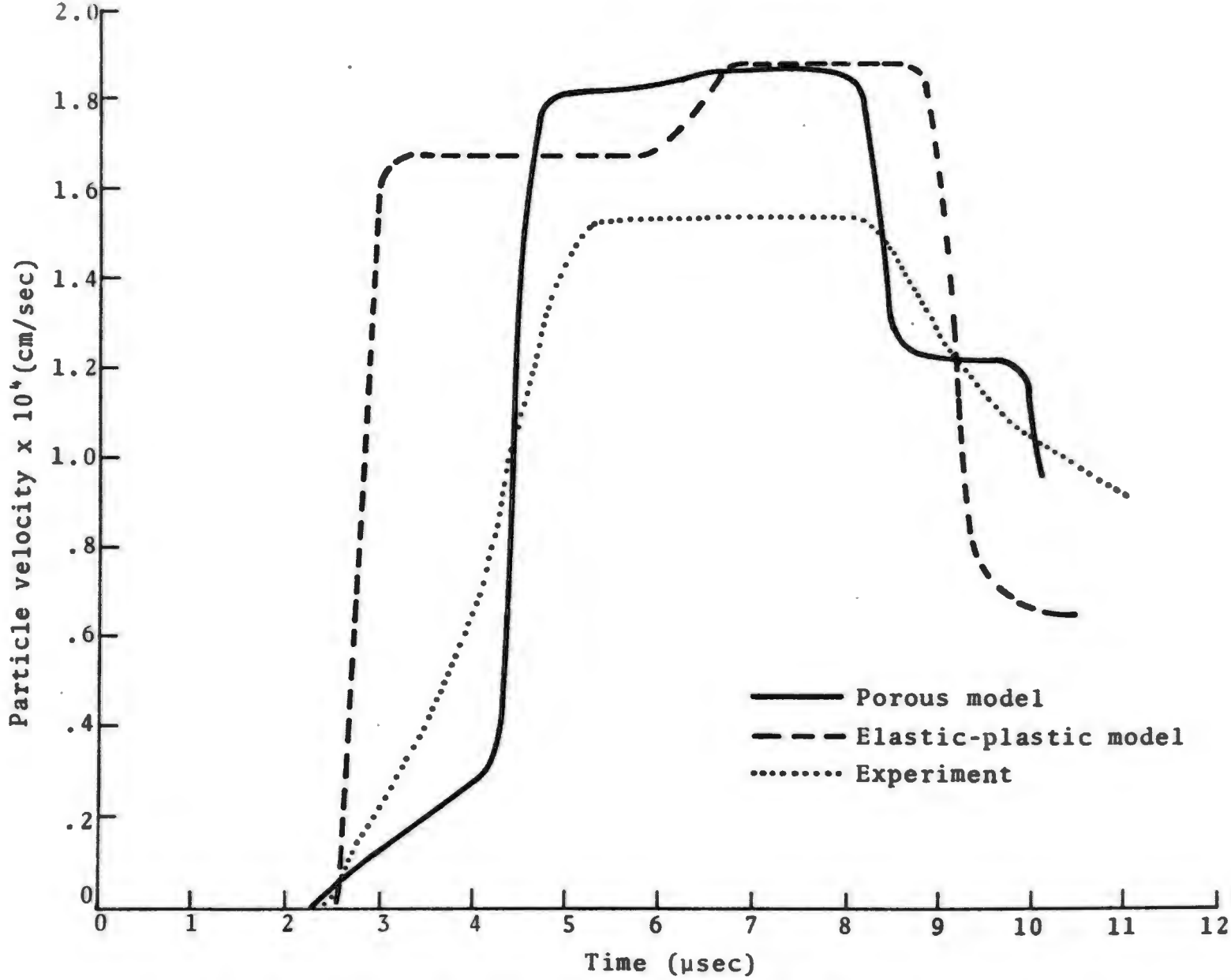

Fig. 13 - Particle velocity histories at depth of 0.303 cm in Plexiglas for Problem No. 4.

with those determined from the calculations. Again, the calculated peak velocities differ substantially from those observed despite the fact that no attenuation is evident in either the experimental or calculated results. Also, the experimental records shown in Figs. 12 and 13 give the release wave profiles and, thus, provide insight into the nature of the unloading process in concrete. From an inspection of these profiles, it becomes evident that neither of the two models correctly describes the unloading process in concrete.

The calculated and observed results for Problems 5, 6, and 7 are given in Figs. 14, 15, and 16, where the stress histories in the polyethylene backup plate at a distance of 0.29 cm from the concrete-polyethylene interface are depicted. The experimental stress histories shown in these figures were obtained with manganin wire gages embedded in the polyethylene. Again, the arrival times were not determined in the experiments, so the experimental records were positioned in the figures in such a manner that the experimental and calculated arrival times agreed. The peak stresses produced in the concrete for Problems 5, 6, and 7 have been estimated by Gregson (see Table II) to be 22, 37.5, and 70.75 kbar, respectively. An elastic precursor is evident in the experimental data for Problem 5 but is not apparent in the data for Problems 6 and 7. The shock velocity-particle velocity data from Gregson's study, depicted earlier in Fig. 3, indicates, however, that the plastic wave speed first exceeds the elastic (ultrasonic) longitudinal wave speed at a particle velocity of about 1.4×10^{5} cm/sec, which corresponds to a stress of approximately 130 kbar. On this basis, a precursor should have been observed in Problems 5, 6, and 7, where the peak stresses were all considerably less than 130 kbar. It is not clear at this time why there is such a discrepancy, although there is some doubt about the ability of the manganin wire gages to resolve the low stresses which arise in the precursor. Despite this, the agreement between the calculated and experimental results for Problems 5 to 7 is better than for the other problems considered in this study.

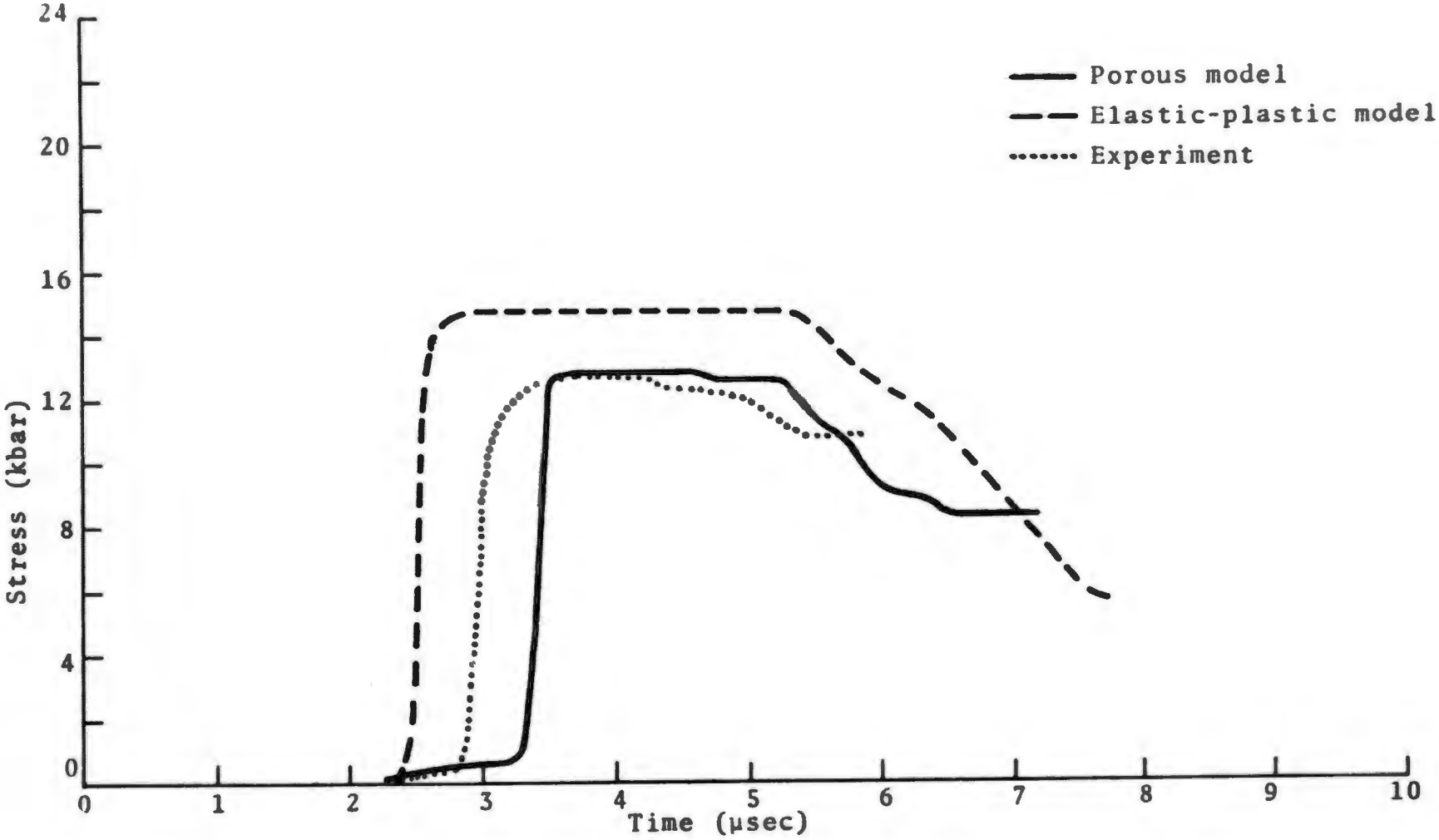

Fig. 14- Stress histories at depth of 0.29 cm in polyethylene for Problem No. 5

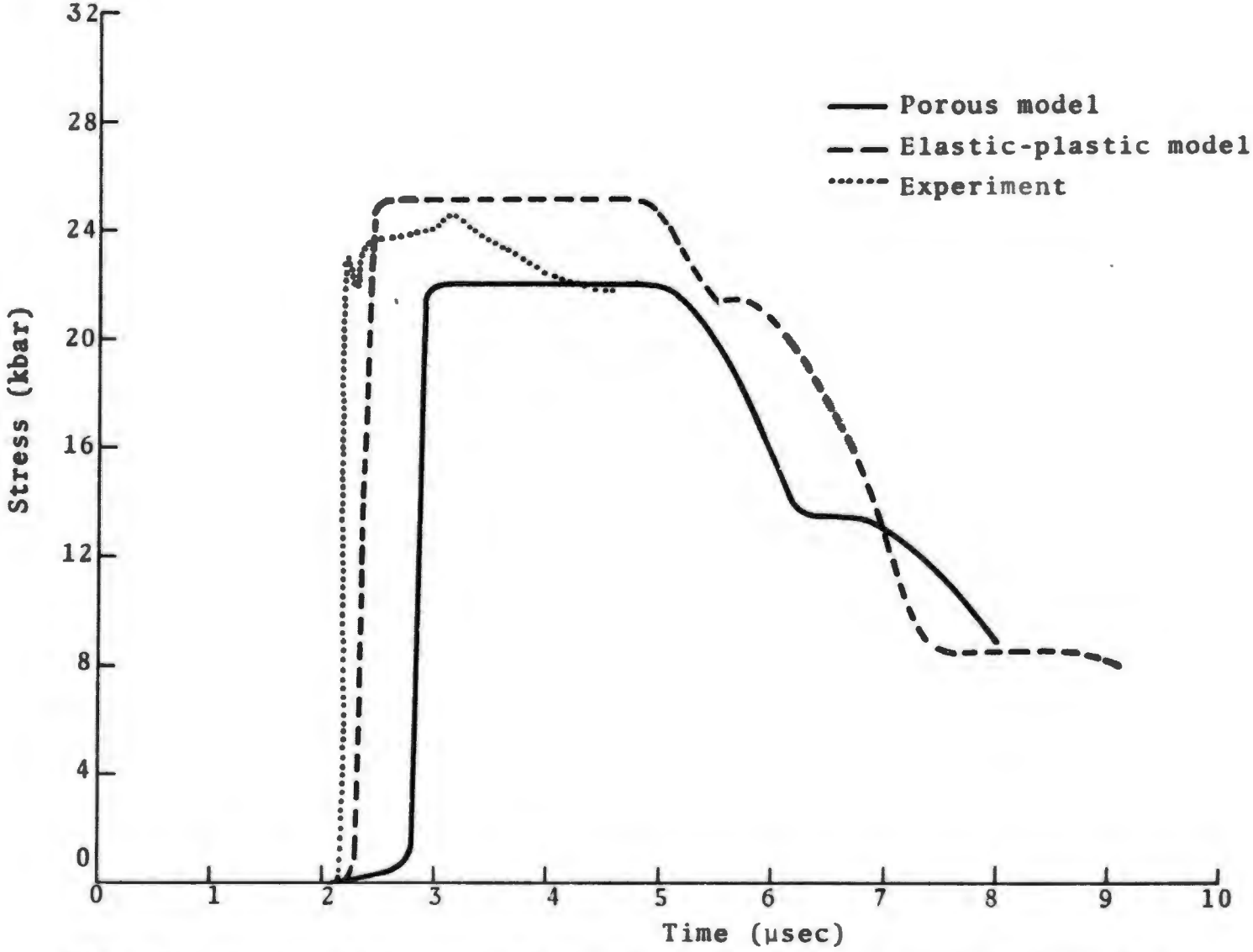

Fig. 15 - Stress histories at depth of 0.29 cm in polyethylene for Problem No. 6

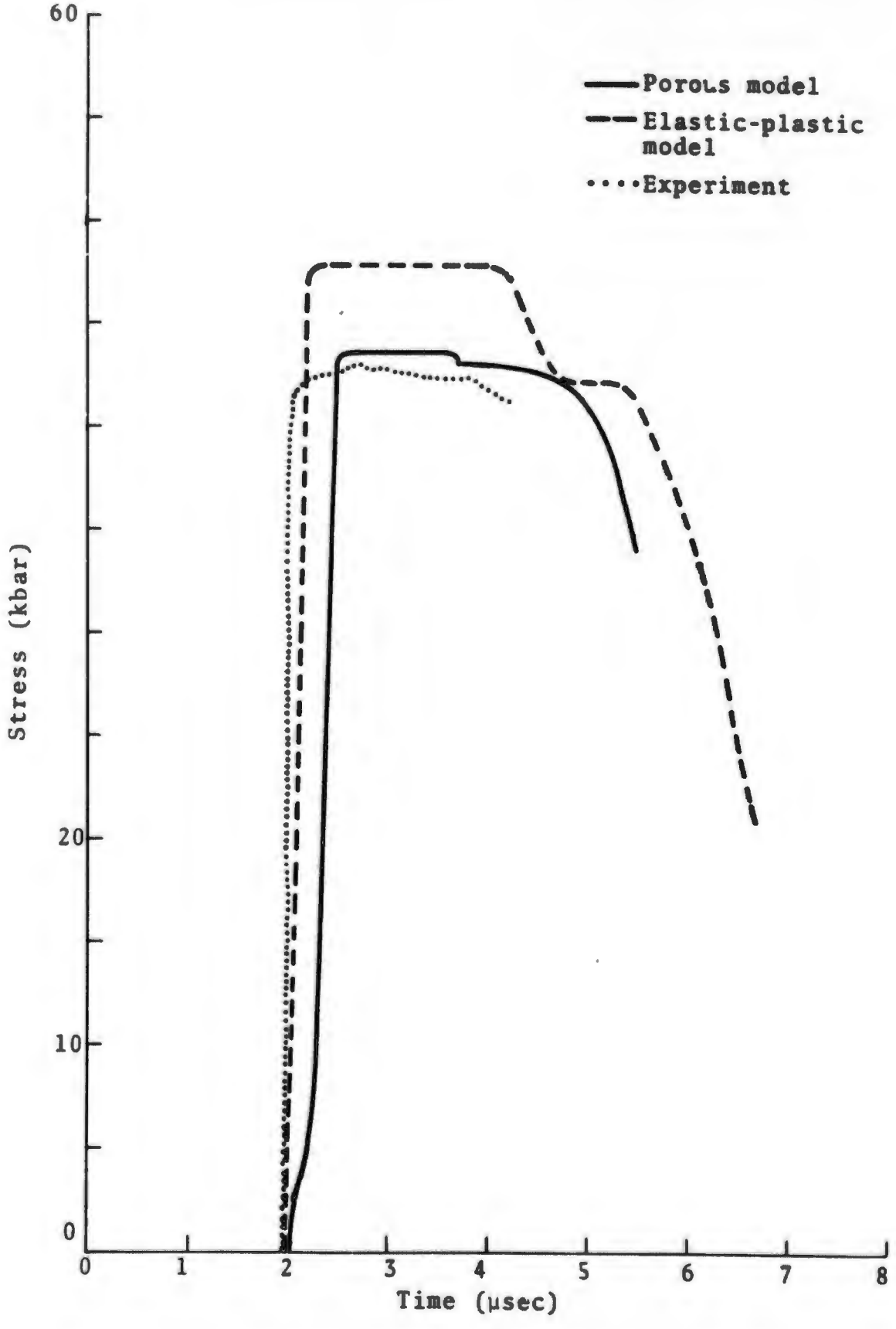

Fig. 16 - Stress histories at depth of 0.29 cm in polyethylene for Problem No. 7.

4. CONCLUSIONS AND RECOMMENDATION

From a review of earlier studies of the dynamic behavior of concrete, it becomes clear that only an initial step has been made toward understanding the complex response characteristics of this technologically important material. While numerous investigations of the static behavior of concrete have been reported in the literature, relatively little attention has been given to its dynamic behavior, particularly in the cases of impulsive mechanical loading and sudden radiation-induced loading. Primary consideration is given to the uniaxial strain configuration in this study because of the analytical convenience it affords in attempting to understand the complex response of this material. Brief recapitulations of the main topics covered in this report are given below together with specific recommendations for avenues of research that should receive attention in future efforts.

Impulsive Mechanical Loading

The recent experimental study by Gregson[19] appears to be the first to address the problem of the response of concrete to shock loading, in the range of stresses of practical importance to the defense community. Although the scope of this program was not sufficiently extensive to provide all of the data required for the development of a realistic constitutive model of concrete, the results obtained nevertheless provide new insight into the dynamic properties of this material. Additional experiments are needed to characterize the Hugoniot in the stress range 0-50 kbar, which is of greatest practical interest. Moreover, since there is a complete absence of data on the attenuation of thin stress pulses in concrete, a systematic study of release wave propagation and attenuation phenomena are required before a realistic constitutive model can be developed.

Radiation-Induced Loading

The most thorough attempt to date to determine the Grüneisen coefficient for concrete has been made by Shea.[24] In this work, the Grüneisen coefficient was obtained for both regular and air-entrained concrete at relatively low doses of radiation, which produced peak pressure well below the elastic limit. At doses higher than those investigated by Shea, there is reason to suspect that, because of the porous nature of concrete, the value of the Grüneisen coefficient will differ substantially from that determined at low doses. Furthermore, most solid materials exhibit a dependence of the Grüneisen coefficient on density and it is reasonable to assume that this is also true of conrete. There is, therefore, a need for controlled, laboratory experiments to provide insight into the dependence of the Grüneisen coefficient for concrete on the density and specific internal energy.

Spallation

Under uniaxial stress conditions, Birkimer[25] determined the spall thresholds of several types of concrete and proposed a theoretical spall criterion which correlated the experimental data very well. Aside from the limited data on spall obtained by Shea,[24] the spall threshold of concrete under uniaxial strain conditions is virtually unexplored. Although no spall threshold was determined in the experiments performed by Gulf General Atomic,[20] there was a clear indication that air entrainment significantly raised the resistance to spall. Additional experimental work, coupled with a corresponding effort to develop a theoretical spall criterion, is needed before spallation thresholds in concrete can be predicted with reasonable accuracy.

Constitutive Modeling

From the studies by Goldsmith, et al.[16] and Pozzo,[17] it appears that the solid-friction model provides a simple and realistic macroscopic description of the dynamic behavior of concrete, at least for stresses not exceeding one kilobar. At much higher stresses, there is some limited indication that the solid-friction model is not realistic.[17] For impulsive loads above one kilobar, there have apparently been no serious efforts, to date, to develop an accurate model of the dynamic response of this technologically important material.

In the analysis of underground test data, and in the design of various defense-related structures, the simple elastic-plastic (von Mises) model has been used in the past to describe the dynamic behavior of concrete. The recent experimental results of Gregson, and the present numerical study, show that the simple elastic-plastic model, as well as the porous model described herein, lack many of the observed response characteristics of concrete; some of these have a strong influence on the ability to correctly calculate the propagation and attenuation features of thin stress pulses. Thus, in the area of defense analysis and design, where an understanding of the response of concrete to short-duration pulses is of vital importance, there is an existing need for a realistic and practicable constitutive model of concrete.

References

1. Newman, K., "The Structure and Properties of Concrete - An Introductory Review," in The Structure of Concrete, A.E. Brooks and K. Newman (Eds.), Cement and Concrete Assn., London, 1968.

2. Slate, R.O., and S. Olsefski, "X-ray for Study of Internal Structures of Microcracking of Concrete," Proc. Am. Concrete Inst., Vol. 60, 1963, p.575.

3. Glucklich, J., "The Effect of Microcracking on Time-dependent Deformation and Long-term Strength of Concrete," in The Structure of Concrete, A.E. Brooks and K. Newman (Eds.), Cement and Concrete Assn., London, 1968, p.176.

4. Ferritto, J.M., "Dynamic Tests of Model Concrete," Naval Civil Engineering Laboratory, TR-65, 1969.

5. Hirsch, T.J., Proc. Am. Concrete Inst., Vol. 59, 1962, p. 427.

6. Powers, T.C., in Chemistry of Cement, Proc. Fourth International Symposium, Washington, D.C., 1960, p.577.

7. Ishai, O., Proc. Am. Concrete Inst., Vol. 59, 1962, p.1365.

8. Kaplan, M.F., Proc. Am. Concrete Inst., Vol. 60, 1963, p. 853.

9. Walker, S., and D.L. Bloem, Proc. Am. Concrete Inst., Vol. 57, 1960-1961, p.283.

10. Blanks, R.F., and C.C. McNamara, Proc. Am. Concrete Inst., Vol. 31, 1935, p.280.

11. Grocell, G.E., and H.E. Davis, Composition and Properties of Concrete, McGraw-Hill, New York, 1956, p.191.

12. Brown, W.S., and S.R. Swanson, "Constitutive Equations for Westerly Granite and Cedar City Tonalite for a Variety of Loading Conditions," University of Utah, Mechanical Engrg. Dept., Report DASA-2473, 1970.

13. Newman, K., and J.B. Newman, Proc. of Conf. on Structures, Solid Mechanics and Engrg. Design in Civil Engrg. Materials, John Wiley, 1969, p. 83.

14. Salch, J.H., W.M. Cegelski, G.R. Danker, and P. Nordin, Response of Construction Materials," (U), TRW Systems Group, Project Officer's Report 6356, Shot Diesel Train, June 1970 (S/RD).

15. Herrmann, W., "Constitutive Equation for the Dynamic Compaction of Ductile Porous Materials," J. Appl. Phys., Vol. 40, 6, 1969, p. 2490.

16. Goldsmith, W., M. Polivka, and T. Yang, "Dynamic Behavior of Concrete," Experimental Mechanics, February 1966, p. 65.

17. Pozzo, E., "Rheological Model of Concrete in the Dynamic Field," Meccanica, Vol. 5, June 1970, p. 143.

18. Whittier, J.S., and A. Ching, "Dispersion of an Elastic Step Pulse Propagating in Concrete - Preliminary Test Results," Aerospace Corp., El Segundo, Report TOR-0066 (5240-30)-2, July 1969.

19. Gregson, V.G., Jr.,"A Shock Wave Study of Fondu-Fyre WA-1 and a Concrete," General Motors Materials and Structures Laboratory, Report MSL-70-30, 1971.

20. Wasser, E.L., "High Explosive Test Program for HRSD," Gulf General Atomic, Report GACD-10104(4-70), April 1970.

21. Skidmore, I.C., Atomic Weapons Research Establishment, Aldermaston, England, Private communication.

22. Suguichi, H., and B.R. Sullivan, "Determination of the Hugoniot Equation of State of Grout," U.S. Army Engineer Waterways Experiment Station, Technical Report No. 6-669, August 1967.

23. Masso, J.F., "Response of Construction Materials, Hudson Moon Experiment 8.35" (U), Systems, Science and Software Report 3SCR-696, June 1971 (S/RD).

24. Shea, J.H., Physics International, private communication.

25. Birkimer, D.L., and R. Lindermann, "Dynamic Tensile Strength of Concrete Materials," Am. Concrete Inst. J., Vol. 68, 1971, p. 47.

26. Green, S.J., et al., "Constitutive Relations for Concrete at Intermediate Pressure Levels," Terra Tek, Inc., Report TR 71-34, 1971.

27. Fisher, R.H., R.A. Cecil, and G.A. Lane, "RIP, A One-Dimensional Material Response Code," Systems, Science and Software, Report 3SR-751, August 1971.

28. Kohn, B.J., "Compilation of Hugoniot Equations of State," Air Force Weapons Laboratory, Kirtland AFB, Report AFWL-TR-69-38, April 1969.

29. Barker, L.M., and R.E. Hollenbach, "Shock-Wave Studies of PMMA, Fused Silica and Sapphire," J. Appl. Phys., Vol. 41, 10, September 1970, p. 4216.

30. Holt, A.C., M. Carroll, and A. Kusubov, "A Simple Constitutive Relation for Porous Materials," Lawrence Radiation Laboratory, Univ. of Calif., Livermore, Report UCRL-74057, March 1971.

Unclassified
Security Classification

DOCUMENT CONTROL DATA - R & D

(Security classification of title, body of abstract and indexing annotation must be entered when the overall report is classified)

1. ORIGINATING ACTIVITY (Corporate author)

Systems, Science and Software
P.O. Box 1620
La Jolla, California 92037

2a. REPORT SECURITY CLASSIFICATION
Unclassified

2b. GROUP

3. REPORT TITLE

(6) The Dynamic Behavior of Concrete,

4. DESCRIPTIVE NOTES (Type of report and inclusive dates)

(9) Topical Report, Apr[redacted] — Aug[redacted]71,

5. AUTHOR(S) (First name, middle initial, last name)

(10) Harold E. Read
Colin J. Maiden

(12) 60p.

6. REPORT DATE

(11) Aug[redacted]71

7a. TOTAL NO. OF PAGES
56

7b. NO. OF REFS
30

8a. CONTRACT OR GRANT NO.

(15) ~~SAMSO~~ FO 4701-70-C-0194

b. PROJECT NO.

c.

d.

9a. ORIGINATOR'S REPORT NUMBER(S)

(14) 3SR-707

9b. OTHER REPORT NO(S) (Any other numbers that may be assigned this report)

10. DISTRIBUTION STATEMENT

Approved for public release; distribution unlimited

11. SUPPLEMENTARY NOTES

12. SPONSORING MILITARY ACTIVITY

Space and Missile Systems Organization
United States Air Force
Norton Air Force Base, California

13. ABSTRACT

A review of the current knowledge of the dynamic behavior of concrete is given. Summaries of related research studies performed by the academic community and the following defense contractors are presented: Aerospace Corporation, General Motors, Gulf General Atomic, Physics International, Terra Tek, and TRW. Particular attention is given in this review to rapid, impulsive loading of concrete resulting from mechanical impact and sudden exposure to radiation. Shock wave propagation and spallation phenomena are discussed. The coefficients for an existing constitutive model of a porous material are determined for a particular concrete. Numerical results based on this model and on an existing elastic-perfectly plastic model are given for several shock loading problems, and comparisons with corresponding experimental data are presented. The results indicate that neither model is adequate enough to predict with reasonable accuracy the shock effects in concrete. Recommendations for future research in these areas are given.

338 507

DD FORM 1 NOV 68 1473

Unclassified
Security Classification

14 KEY WORDS	LINK A		LINK B		LINK C	
	ROLE	WT	ROLE	WT	ROLE	WT
Materials Science Concrete Shock Waves Wave Propagation Spallation Porous Materials						